④

AFGL-TR-89-0065

SURFACE WAVE RAY TRACING AND M_S:YIELD DETERMINATION IN A
LATERALLY HETEROGENEOUS EARTH

Yuehua Zeng
Ta-liang Teng
Keiiti Aki

University of Southern California
Department of Geological Sciences
University Park
Los Angeles, CA 90090

February 1989

Final Report
7 January 1987-31 December 1988

DTIC
ELECTE
JUL 11 1989
S D
9 E

AIR FORCE GEOPHYSICS LABORATORY
AIR FORCE SYSTEMS COMMAND
UNITED STATES AIR FORCE
HANSCOM AIR FORCE BASE, MASSACHUSETTS 01731-5000

JAMES F. LEWKOWICZ
Contract Manager
Solid Earth Geophysics Branch
Earth Sciences Division

JAMES C. BATTIS
Acting Chief
Solid Earth Geophysics Branch
Earth Sciences Division

FOR THE COMMANDER

DONALD H. ECKHARDT, Director
Earth Sciences Division

REPORT DOCUMENTATION PAGE

Form Approved
OMB No. 0704-0188

1a. REPORT SECURITY CLASSIFICATION	1b. RESTRICTIVE MARKINGS
Unclassified	

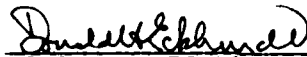| 2a. SECURITY CLASSIFICATION AUTHORITY	3. DISTRIBUTION/AVAILABILITY OF REPORT
	Approved for public release; distribution
2b. DECLASSIFICATION/DOWNGRADING SCHEDULE	unlimited

4. PERFORMING ORGANIZATION REPORT NUMBER(S)	5. MONITORING ORGANIZATION REPORT NUMBER(S)
	AFGL-TR-89-0065

6a. NAME OF PERFORMING ORGANIZATION	6b. OFFICE SYMBOL (If applicable)	7a. NAME OF MONITORING ORGANIZATION
University of Southern California		Air Force Geophysics Laboratory

6c. ADDRESS (City, State, and ZIP Code)	7b. ADDRESS (City, State, and ZIP Code)
Department of Geological Sciences University Park Los Angeles, CA 90089	Hanscom AFB Massachusetts 01731-5000

8a. NAME OF FUNDING/SPONSORING ORGANIZATION	8b. OFFICE SYMBOL (If applicable)	9. PROCUREMENT INSTRUMENT IDENTIFICATION NUMBER
		F19628-87-K-0018

8c. ADDRESS (City, State, and ZIP Code)	10. SOURCE OF FUNDING NUMBERS			
	PROGRAM ELEMENT NO.	PROJECT NO.	TASK NO.	WORK UNIT ACCESSION NO.
	61101E	7A10	DA	CR

11. TITLE (Include Security Classification)
Surface Wave Ray Tracing and M_S: Yield Determination in a Laterally Heterogeneous Earth

12. PERSONAL AUTHOR(S)
Yuehua Zeng, Ta-liang Teng; Keiiti Aki

13a. TYPE OF REPORT	13b. TIME COVERED	14. DATE OF REPORT (Year, Month, Day)	15. PAGE COUNT
Final Report	FROM 1/7/87 TO 12/31/88	1989 February	62

16. SUPPLEMENTARY NOTATION

17.	COSATI CODES		18. SUBJECT TERMS (Continue on reverse if necessary and identify by block number)
FIELD	GROUP	SUB-GROUP	surface waves; ray tracing; yield determination, Arctic region

19. ABSTRACT (Continue on reverse if necessary and identify by block number)

Pure path Rayleigh wave group velocities for 24 regional grids inside the Arctic have been obtained from 74 mixed path measurements. The vertical shear wave velocity structures under these 24 grids were then determined according to their pure path group velocity dispersion data. This result indicates that the crustal shear wave velocity in the Arctic region is generally lower than the world-wide average. In addition, a typical mid-ocean ridge structure was clearly shown under the Nansen Ridge. We also found an abnormally high upper mantle shear wave velocity under the Alpha Ridge and Makarov Basin, and low velocity beneath the Canadian Arctic Islands. In general, our inversion result agrees with the known tectonics in the Arctic region. To further check the validity of our result, we have computed synthetic Rayleigh waves and a comparison with our observations shows very good agreement.

20. DISTRIBUTION/AVAILABILITY OF ABSTRACT	21. ABSTRACT SECURITY CLASSIFICATION
☐ UNCLASSIFIED/UNLIMITED ☐ SAME AS RPT. ☐ DTIC USERS	Unclassified

22a. NAME OF RESPONSIBLE INDIVIDUAL	22b. TELEPHONE (Include Area Code)	22c. OFFICE SYMBOL
James Lewkowicz	(617) 377-3028	AFGL/LWH

DD Form 1473, JUN 86   Previous editions are obsolete.   SECURITY CLASSIFICATION OF THIS PAGE

Unclassified

SURFACE WAVE RAY TRACING AND M$_S$:YIELD DETERMINATION IN A LATERALLY HETEROGENEOUS EARTH

University of Southern California
Center for Earth Sciences
Los Angeles, CA 90089-0740

Name of Contractor: University of Southern California

Contract Number: F19628-87-K-0018

Contract Period: January 7, 1987 to December 31, 1988

Principal Investigators: Ta-liang Teng
Professor of Geophysics
(213) 743-6124

Keiiti Aki
W. M. Keck Foundation Professor of Geophysics
(213) 743-3510

Sponsored by

Defense Advanced Research Projects Agency (DOD)
Defense Sciences Office, Geophysical Sciences Division
DARPA/ARPA Order No.

February, 1989

iii

Introduction

The Arctic region (Fig. 1) is a tectonically interesting area with complex crust and upper mantle structure. Surrounded by continental shelves with the East Siberian Shelf, Laptev Shelf, Kara Shelf and Beaufort Shelf on its east side, and the Chukchi Shelf, Beaufort Shelf and Greenland on its west side, the crust beneath the Arctic Ocean floor is composed of oceanic basins and mid-ocean ridge systems. These oceanic basins, including the Canada Basin, Makarov Basin, Fram Basin and Nansen Basin, are observed in near-parallel positions across the Arctic Ocean and are separated by the Alpha Ridge, Lomonosov Ridge and Nansen-Gakkel Ridge.

In spite of the difficulties in exploring the Arctic area in detail, generalized tectonic histories have been proposed by many researchers (Mair and Forsyth, 1982; Sweeney, Weber and Blascco, 1982; Fugita and Newberry, 1982; Harland, 1973; Sweeney, Irving and Gener, 1978). In their studies, it is suggested that the Canada Basin may have formed 125-190 m.y. ago by a counterclockwise rotation of Arctic Alaska away from the Canadian Arctic Islands. The flanking Alpha and Lomonosov ridges may originally have been part of the same continental block and were separated by continental stretching rather than simple sea floor spreading to form the Makarov Basin. This continental block was sheared from Eurasia along a Trans-Arctic

1

left-lateral shear zone in late Cretaceous which was related to the opening of the Canada Basin, and was separated from Eurasia when the North Atlantic rift system extended to the Arctic region during Early Tertiary time. On the other hand, the Fram Basin and Nansen Basin may have formed about 70 m.y. ago by sea floor spreading along the Nansen-Gakkel Ridge with the opening of the North Atlantic. These studies also suggested that the East Siberian Sea may be floored by oceanic crust left by an incomplete closure between the Arctic Alaska, Siberia, and Omolon.

A number of geophysical studies have investigated the structures of the Arctic by means of gravity, geothermal, geomagnetic, seismic reflection and refraction profiling, and surface wave dispersion methods (Johnson and Sweeney, 1982; Chan and Mitchell, 1985). But a detailed crust and upper mantle study of this region as a whole has not been completed. Strong lateral heterogeneity in this region is not only suggested by its tectonic complexity, but also demonstrated by seismological observations. In an earlier study, Zeng et al. (1986) have found remarkable focusing and defocusing effects of surface waves propagating across this region. In order to improve our understanding of Arctic tectonics and to provide an overall quantitative description for the lateral heterogeneity properties, we have conducted a detailed Rayleigh wave group velocity dispersion study for the Arctic region.

2

In this surface wave dispersion study, we have used the Rayleigh wave data for earthquakes from Alaska, Aleutian Islands and Northeast Siberia recorded at the WWSSN stations around the Arctic. Using the surface wave dispersion method introduced earlier (Feng and Teng, 1983b), we divided our study into three steps. First, we measured the mixed-path Rayleigh wave group velocity from hand digitized seismograms by a matched-filtering process. We then divided the region of interest into smaller subdivisions in which lateral homogeneity is assumed, and determined pure-path group velocities for these subdivisions from the mixed-path measurement by a stochastic inversion method. Third, we obtained the vertical shear wave velocity structure from the pure-path data for each subdivision. Following these steps, we studied the lateral variations of the Arctic crustal and upper mantle structure and tried to interpret the variations in terms of tectonic evolution in this region. In addition, we have computed Gaussian beam synthetics for surface wave propagation across the Arctic region using our inversion result. The synthetic seismograms were then compared with the observed seismograms to test the validity of the Arctic crust and upper mantle model obtained from the inversion.

Data Acquisition and Analysis

To obtain the long-period Rayleigh waves with paths across the Arctic region, we searched the earthquake catalog for all

3

events above 50 degrees north latitude with magnitude from 5.5 to 6.5 mainly during the period from 1979 to 1985. A total of 118 events were found. Among these events, we eliminated ones with poor signal-to-noise ratio and redundant path coverage. Seismograms of these events recorded at the WWSSN stations (see Table 1) were obtained from the film chips. The selected events are listed in Table 2, from which 102 seismograms were chosen for hand digitization. A typical example of these seismograms is shown in Figure 2a, which was recorded at station COP for an event some 8,000 km away. The beating of this wave train suggests strong lateral heterogeneity along the path.

The hand digitized seismograms were then corrected for the instrument response according to Hagiwara (1958), in which the coupling effect between seismometer and galvanometer is neglected. These corrected seismograms were used in the matched-filtering process (Feng and Teng, 1983a) to obtain the group arrival times. In this matched-filtering process, we first used the display-equalized filtering process (Nyman and Landisman, 1977) to obtain our preliminary group arrival time, and then we used these preliminary results to obtain the optimal filter parameters for the optimal bandwidth filtering process (Inston et al., 1971; Cara, 1973; Feng and Teng, 1983). The final group arrival times were used in the mixed path group velocity calculations. The correction for the source delay was not applied since its effects are small in view of the magnitudes of events and

4

epicentral distances used in this study. A sample of the dispersion curve is shown in Fig. 2b for the seismogram shown in Fig 2a.

According to the results of the matched-filtering process, we further sorted our seismograms by deleting data sets with large scatter in the group velocity measurements. A total of 74 wave paths with good group velocity measurements and proper path coverage over the Arctic region were finally selected from the 102 seismograms (see Table 3). The Arctic region was then subdivided into 24 region grids, each of an area of 5 to 10 degrees in dimension (Fig. 3a). Within each region grid lateral homogeneity is assumed. These region grids were made on a rotated world map with pole located at zero latitude and longitude. We have divided these grids based on both the Arctic tectonic features and our selected ray path coverage. For instance, we defined the grids so that they are mainly composed of either oceanic path or continental path, and we made the mesh size larger in the region with relatively poorer path coverage. Map views of both the grids and Rayleigh wave ray path coverage are shown in Fig. 3a and 3b, respectively.

The stochastic inversion technique (Franklin, 1970) was used to determine the pure path group velocities for our regional subdivision according to the formula

$$t_i(\omega) = \sum_j D_{ij} / U_j(\omega)$$

where t_i is the group arrival time for path i at frequency ω, D_{ij} is the distance of path i contained in grid j, and $U_j(\omega)$ is the pure path group velocity for grid j. To carry out the stochastic inversion, we first performed a simple least squares inversion to estimate the parameters needed for stochastic inversion, such as the noise variance, the model variance and the average inverse group velocity. The noise variance was estimated as the sum of squares of time residuals for each path divided by the number of degrees of freedom. The model variance was estimated as the mean square of the inverse pure path group velocity minus their average value. The initial value of group velocity for the stochastic inversion is taken as the average value from this least squares inversion. These parameters were then used in the standard procedure of the stochastic inversion to obtain final pure-path group velocities.

Examples of the resolution matrix and covariance matrix of the stochastic inversion are shown in Fig. 4a and Fig. 4b. In these plots, the line interval is 1 for the resolution matrix plot and $0.01 \times (\overline{U}^{-1})^2$ for the variance matrix plot. These plots correspond to the period of 41.58 sec. The root mean square residual time for this period is 30.3 sec. Table 4 listed the standard error of the pure-path group velocity for this period. From Table 4, we see that the average standard error for this period is around 0.1 km/sec. According to the empirical equation of Knopoff and Schwab (1968), the error due to source delay should be less than

6

0.02 km/s for the epicentral distance range in our study. The group velocity measurement error introduced from the matched-filtering process should be less than 0.02 km/s (Feng and Teng, 1983a). Taking the values of 3.5 sec for travel time error due to epicentral determination, 1.5 sec for origin time error, 1.75 sec for finiteness error and 2.0 sec for digitization errors (Chan and Mitchell, 1985), and calculating the group velocity errors due to each source by using the relation given by Forsyth (1975)

$$\Delta U_e = E_i U^2 / D$$

where ΔU_e is the group velocity error due to E_i, E_i is the time error due to source i, U is the group velocity, and D is the epicentral distance, a total error of 0.02 km/sec was estimated for the group velocity of 3.6 km/sec and epicentral distance of 4000 km. Thus an error of 0.05 km/sec was obtained for all the sources indicated above. Comparing this value with the average standard error obtained from our stochastic inversion, a difference of 0.05 km/sec in the error was unexplained. We suspect that this additional error was introduced from our regionalization modeling and great circle path assumption for the Rayleigh wave propagation.

Finally, our pure path results were used for the layered shear wave velocity structure inversion for each region grid. To avoid any artificial features introduced from the initial model, we

have decided to use the same model as our initial model for all blocks. This model was obtained by averaging some continental and oceanic shear wave models from earlier studies (Feng and Teng, 1983b; Yu and Mitchell, 1979; Seneff, 1978; Kanamori and Abe, 1968; Harkrider and Anderson, 1966). The generalized inversion method is used for our shear wave velocity modeling study. The program we have used for the inversion was modified from the one originally written by Harkrider and later modified by Rodi. This program used a surface wave algorithm formulated by Harkrider (1964) and a method for computing group velocity partial derivatives given by Rodi et al. (1975).

Results and Discussion

The pure path group velocity models obtained from our stochastic inversion were contoured in Fig. 5a and Fig. 5b for periods of 19.9 sec and 41.6 sec respectively. The contour interval is 0.09 km/sec. In the contour plot for 19.9 sec (Fig. 5a), we see high group velocities for the oceanic blocks and low group velocities for the continental shelves. This phenomenon is generally expected at short periods. A close examination of this plot reveals a relatively lower group velocity for the Canada Basin and Alpha Ridge. These features are consistent with previous findings that the Canada Basin is the oldest Basin in the Arctic ocean with a thick layer of sediments and that Alpha Ridge in general has a crust of continental structure (Mair and Forsyth,

8

1982; Vogt et al., 1982; Kovacs et al., 1982). From the contour plot for 41.6 sec period (Fig. 5b), a relatively higher group velocity contour was found for grid 13. This grid includes Alpha Ridge, Makarov Basin and a portion of Lomonosov Ridge. Since a longer period surface wave samples a deeper portion of the earth, it indicates a high velocity layer located under this grid in the upper mantle. We will come back to this point shortly.

Before we interpret the shear wave velocity models obtained in the previous section, we would like to first address the resolution kernels associated with our starting model at several depth ranges. Figure 6 is a plot of the resolution kernels. Since we used the same starting model and period range, the resolution kernel is basically the same for all grids. This resolution kernel shows the best resolution provided by our data for depths ranging from 10 to 50 km. The peak of the resolution kernel decreases and the width increases with increasing depth, indicating deteriorating resolution with depth. The resolution is also poor at shallow depths above 3 to 5 km for lack of short-period data. So we will limit our discussion to the depth range between 5 and 250 km.

According to Sweeny et al. (1982), the Moho in the Arctic ocean was defined by a P wave velocity change from 6.6 to 8.3 km/sec. Following Nafe's (1970) empirical relation, this change corresponds to a S wave velocity change from 3.75 to 4.5 km/sec.

Although the seismic discontinuity cannot be located effectively using the surface wave inversion method, we approximated it by the contour level of 3.75 km/sec. We modified the model we obtained in the previous section by passing a moving average over a 6 km range with an increment of 3 km. Fig. 7 is a series of cross section maps of crustal structure from the North American side to the North Eurasia side. Location is indicated by the region grid numbers at the top of the cross-sections. The validity of our process can be shown by comparing them with known surface geology. As was pointed out before, the Canada Basin was formed around upper Jurassic or early Cretaceous time. The oceanic crust below the Canada Basin is much thicker and older than that below the Makarov and Eurasia basins (Mair and Forsyth, 1982; Vogt et al., 1982). In our grid division, the Canada Basin is included in grid 7, the Makarov Basin in grid 13, and the Eurasia Basin in grid 14. A comparison of the crustal thickness between grid 7, grid 13 and grid 14 in Fig. 7 supports this conclusion. The Barents shelf offers another example. This area has been carefully studied by Chan and Mitchell (1985). Their study revealed that the crustal thickness of the central shelf is about 37 km and it decreases to only around 23 km in the western shelf. Since the western region of the shelf is covered by our grids 18 and 21 and the rest of the shelf is covered by grids 19 and 22, we found by examining our plot that the crustal thickness below the Barents shelf is more than 30 km at its eastern side and generally thins to the west. So

we may say that our result roughly captures the main crustal structure in the Arctic region. In addition, the overall picture suggests that the crust is around 20 to 40 km thick in the Arctic region.

Fig. 8 is a series of cross-sections. The upper mantle structures are given by velocity contours from the North American side to the North Eurasia side for all grids except grid 1, 2, 24. Fig. 9 gives similar cross-sections, but perpendicular to those given in Fig. 8. A close examination of these figures reveals a thick layer with abnormally high upper mantle velocity located under grid 13. The same phenomenon has been pointed out previously from the long period group velocity contour map. Fig. 10 shows a vertical profile of the shear wave velocity model for grid 13. The abnormally high upper mantle velocity is clearly depicted in this figure. This grid is mainly covered by the Alpha Ridge, and partly by the Makarov Basin and the Lomonosov Ridge. Theories have been proposed to explain the origin of the Alpha Ridge (Coles et al., 1978; Delaurier, 1978; Sweeny et al., 1978a, b; Vogt et al., 1981b; Taylor et al., 1981; Sweeny et al., 1982). It is generally agreed that the ridge was once a subsided continental fragment, and then changed to an extinct oceanic spreading center. The recovery of microfossils up to 70 m.y. old from the ridge crest sediments indicates that it ceased spreading by late Cretaceous and is only a fossil spreading center at present (Sweeny, 1981). The abnormally high upper mantle velocity resolved from our

11

Rayleigh wave dispersion inversion also indicates that this region no longer possesses the characters of a spreading center.

The Nansen Ridge is included in grids 14 and 18. From the contour plot in Fig. 9 and shear wave velocity profile in Fig. 11, we can see that below the crustal lid, there is a well-developed low velocity zone. This suggests the existence of partial melting in this zone consisting of hot mantle material pushing the ridge apart. The extensive aeromagnetic investigation by Soviet, Canadian, and U.S. Navy research groups have found typical sea-floor spreading type magnetic anomalies in this region (Vogt et al., 1979). It also suggests that the Nansen Ridge began spreading about 70 m.y. ago and separated the Lomonosov Ridge from Barents shelf and formed the Fram Basins.

In the region covered by grids 11 and 16, our result shows a profound low shear wave velocity structure in the crust and upper mantle (see Fig. 8 and Fig. 12). In view of the ray path coverage in this region, our result is probably influenced mainly by the structure under Queen Elizabeth Island, Ellesmere Island, Sverdrup Island and Baffin Bay area. It has been suggested that there is a very long-lived hot spot underneath Sverdrup Island (Balkwill, 1978). Additionally, seismic studies indicate that it is a tectonically active region weakened by deviatoric horizontal extension in a direction perpendicular to the continental margin (Fujita et al, 1986). We suspect that this region is still undergoing

12

a mantle pluming process which may be responsible for its present low velocity in the upper mantle.

A comparison of grids 7 and 20 shows that the crust and upper mantle shear wave velocities are quite similar between the Canada Basin and the eastern part of Greenland (see Fig. 13). Both grids have a 30 km thick crust, and are underlain by a 50 km thick upper mantle high shear wave velocity layer. Beneath the upper mantle high velocity layer, there is a well developed asthenosphere from the depth of 100 km to 250 km.

In addition, we have taken an average between depths of 5 and 30 km of the shear wave velocity model obtained from the Rayleigh wave dispersion inversion over all grids. By subtracting these values from the initial velocities, we have found a difference of 0.14 km/sec for the depth from 5 to 10 km, a difference of 0.33 km/sec from 10 to 20 km, and a difference of 0.31 km/sec from 20 to 30 km. This difference indicates that the average crustal shear wave velocity in the Arctic region is much lower than that of other similar oceanic and stable continental regions of the world. This is probably the consequence of intensive tectonic evolution that deformed and fractured this region.

Synthetic Surface Waves

The Gaussian beam method was applied to evaluate the effects of lateral heterogeneity on surface waves propagating

13

across the Arctic region. The initial model was selected using Jordan's (1981) 5 degree by 5 degree tectonic regionalization and Rosa's (1986) surface wave velocity data. We replaced this initial model of the Arctic region by our inversion result to obtain an improved surface wave velocity model. Using this improved model, global surface wave ray maps for 20 sec period were generated for the source of the nuclear test site in Novaya Zemlya. Synthetic seismograms were also generated for the WWSSN stations located in the United States with the same wave period. The program we used for these synthetic calculations was originally written by Yomogida (1985) and then modified by us. Figure 14 is a plot of the global surface wave ray map based on our final model. The synthetic seismograms were plotted in Figure 15 for the initial model and Figure 16 for the final model. Remarkable focusing and defocusing effects were found in surface wave propagations across Arctic for both models. These results were then compared with the observations shown in Figure 17. These observed seismograms were obtained for the same seismic stations and source location. There are some problems in the calculated seismograms from our final model at stations 15 and 16. This is due to refractive bending of rays at the artificial boundary created when we put our inversion result into the initial model. In spite of that, synthetics from our final model give a better fit to the observed seismograms than that from the initial model.

We realize there are large discrepancies between computed and observed seismograms due to some simplifications made in our modeling. For example, we used a Gabor wavelet as the source time function for each beam and calculated its travel time according to our velocity models for the central period of that wavelet. In reality, the source time function is much more complicated than what have been assumed and the wavelet will disperse along its way from source to stations. This may be one reason for the differences between computed and observed wave trains. In our synthetics, we also used a relatively smooth structure comparing to the real situation. As pointed out by the result of Chiou and Mitchell (1986) for the Arctic Islands, there are large variations within a region assumed to be uniform in our model which is limited by the resolution of our data. Strong inhomogeneity was also suggested by the beating phenomenons in our observations. Our velocity models across the North America were based on Jordan's tectonic regionalization (1981) which gave additional simplification to the complicated reality. In this sense, we could not guarantee that our synthetics will reproduce exactly what are observed. Nevertheless, our models still well reflect the observed focusing and defocusing phenomenon.

Conclusion

In this study, we have divided the Arctic region into 24 regional grids. According to this division, a detailed Rayleigh

15

wave dispersion study of the crust and upper mantle structure in the Arctic region was carried out. From the structure inversion results, we mapped the thickness of crustal layer in this region. Although it is not an detailed description, the general features have been captured We found that the crustal shear wave velocity in this region is generally lower than the average shear wave velocity in the other similar oceanic and stable continental regions. By comparing the upper mantle shear wave velocity structures in this area, we found an abnormally high velocity for grid 13 and a low velocities for grids 11 and 16. Since grid 13 mainly covers the Alpha Ridge, this abnormally high velocity supports the conclusion that it is now a fossil spreading center. The low velocities in grids 11 and 16 might imply some kind of weakening process occurring in this area. The result also shows that the upper mantle underneath grids 14 and 18 are characterized by typical oceanic ridge structures. It is consistent with the tectonic activity of the Nansen Ridge. In addition, we found that the structure below the Canada Basin is continental in nature. We also computed Gaussian beam synthetic surface waves using this inversion result as well as the results of others. The synthetics based on our inversion result agree with the observed seismograms better than those for other models. In general, our results reflect the tectonics in the Arctic region and provide additional constraints for this area.

Acknowledgement

References

Balkwill, H. R., Evolution of Sverdrup Basin, Arctic Canada. Am. Assoc. Pet. Geol. Bull., 62: 1004-1028, 1978.

Cara, M., Filtering dispersed wave trains, Geophys. J., 33, 65-80, 1973.

Chan W. W. and B. J. Mitchell, Surface wave dispersion, crustal structure, and sediment thickness variations across the Barents shelf, Geophys. J. R. Astr. Soc., 80, 329-344, 1985.

Chiou, S.-J. and B. J. Mitchell, Regional variations in the crustal structure of Northern Canada from surface wave dispersion, Journal of Geodynamics, 6, 53-69, 1986.

Coles, R. L., W. Hannaford and G.V. Haines, Magnetic anomalies and the evolution of the Arctic, In: J. F. Sweeney (editor), Arctic Geophysical Review, Publ. Earth Phys. Branch, 45: 51-66, 1978.

De Laurier, J., Magnitic anomalies and the evolution of the Arctic. In: J. F. Sweeney (Editor), Arctic Geophysical Review, Publ. Earth Phys. Branch, Dep. Energy, Mines Resour., Ottawa, 45-4: 87-90, 1978.

Feng, C. C., and T. L. Teng, An error analysis of FTAN, Bull. Seismol. Soc. Am., 73, 143-156,1983a.

Feng, C. C. and T. L. Teng, Three-dimensional crust and upper mantle structure of the Eurasian continent, J. Geophys. Res., 88, 2261-2272, 1983b.

Flatte S. and R. S. Wu, Small-scale structure in the lithosphere and asthenosphere deduced from arrival-time and amplitude fluctuations at NORSAR, J. Geophys. Res., 93, 6601-6614, 1988

Franklin, J. N., Well-posed stochastic extensions of ill-posed linear problems, J. Math. Anal. Appl., 31, 682-716, 1970.

Forsyth, D. A., The early structural evolution and anisotropy of the oceanic upper mantle, Geophys. J. R. Astr. Soc., 43, 103-162, 1975.

Fujita, K., D. B. Cook, H. Hasegawa, D. Forsyth and R. Wetmiller, Seismicity and focal mechanisms of the Arctic region and the North American plate boundary in Asia, in Grantz, A.,

Johnson, G. L., and Sweeny, J. F., eds., The Arctic Ocean region, The Geology of North America, V. L: Boulder, Geological Society of America, ch. 6, 1986.

Harland, W. B., Mesozoic geology of Svalbard, In: M. G. Pitcher (Editor), Arctic Geology. Am. Assoc. Pet. Geol., Mem., 19: 135-148, 1973a.

Harland, W. B., Tectonic evolution of the Barents Shelf and related plates, In: M. G. Pitcher (Editor), Arctic Geology. Am. Assoc. Pet. Geol., Mem., 19: 599-608, 1973b.

Harkrider, D. C., Surface waves in multi-layered elastic media, I, Rayleigh and Love waves from buried sources in a multi-layered elastic half space, Bull. Seismol. Soc. Am., 54, 627-679, 1964.

Harkrider, D. G., and D. L. Anderson, Surface wave energy from point sources in plane layered earth models, J. Geophys. Res., 71, 2967-2980, 1966.

Hagiwara, T., A note on the theory of electromagnetic seismograph, Earthq. Res. Inst. Bull. Tokyo Univ., 36, 139-164, 1958.

Inston, H. H., P.D. Marshall, and C. Blamey, Optimization of filter bandwidth in spectral analysis of wavetrains, Geophys. J., 23, 243-250, 1971.

Johnson, G. L. and J. F. Sweeney (ed), Structure of the Arctic, Tectonophysics, 89, Special Issue, 1982.

Jordan, T. H., Global tectonic regionalization for seismological data analysis, Bull. Seismol. Soc. Am., 71, 1131-1141, 1981

Kanamori, H., and K. Abe, Deep structure of island arcs as revealed by surface waves, Bull. Earthq. Res. Inst., 46, Tokyo Univ., 1001-1025, 1968.

Knopoff, L. and F. A. Schwab, Apparent initial phase of a source of Rayleigh waves, J. Geophys. Res., 73, 755-760,1968.

Nafe, J. E., Assembled velocity density data, Sea, 4(1), 53-84, 1970.

Nyman, D. C., and M. Landisman, The display equalized filter for frequency-time analysis, Bull. Seism. Soc. Am., 67, 393-404, 1977.

Ostenso, N. A., Geophysical investigations of the Arctic Ocean basin, Geophys. and Polar Res. Center Res. Rep. 4, Univ. Wisconsin, Madison, 124 pp, 1962.

Rodi, W. L., P. Glover, T. M. C. Li, and S. S. Alexander, A fast, accurate method for computing group velocity partial derivatives for Rayleigh and Love modes, Bull. Seismol. Soc. Am., 65, 1105-1114, 1975.

Rosa, J. W. C., A global study on phase velocity, Group velocity and attenuation of Rayleigh waves in the period range 20 to 100 second. Ph.D dissertation, MIT, 1985

Seneff, S., A fast new method for frequency-filter analysis of surface waves: application in the west Pacific, Bull. Seism. soc. Am., 68, 1031-1048, 1978.

Snieder, R., Surface wave scattering theory, Geologica Ultraiectina; Univ. of Utrecht, No. 50, 1987

Sweeney, J. F., E. Irving and J. W. Geuer, Evolution of the Arctic Basin, In: J.F. Sweeney (Editor), Arctic Geophysical Review. Publ. Earth Phys. Branch, 45: 91-100, 1978.

Taylor, P. T., L. C. Kovacs, P.R. Vogt and G. L. Johnson, Detailed aeromagnetic investigation of the arctic Basin, 2. J. Geophys. Res., 86: 6323-6333, 1981.

Vogt, P. R., P. T. Taylor, L. C. Kovacs and G. L. Johnson, Detailed aeromagnetic investigation of the arctic Basin, J. Geophys. Res., 84: 1071-1089, 1979.

Vogt, P., C. Bernero, L. Kovacs and P. Taylor, Structure and plate tectonic evolution of the marine Arctic as revealed by aeromagnetics. Oceanol. Acta, No. SP:25-40, 1981b.

Yomogida, K. and K. Aki, Waveform synthesis of surface waves in a

laterally heterogeneous Earth by the Gaussian beam method, J. Geophys. Res., 90, 7665-7688, 1985.

Yomogida, K. and K. Aki, Amplitude and phase data inversions for phase velocity anomalies in the Pacific Ocean basin, Geophys. J. R. Astron. Soc., 88, 161-204, 1987.

Yu, G. K. and B. J. Mitchell, Regionalized shear velocity models of the Pacific upper mantle from observed Love and Rayleigh wave dispersion, Geophys. J., 57, 311-341, 1979.

Zeng, Y. H., J. Faulkner, T. L. Teng and K. Aki, Focusing and defocusing of Rayleigh waves from USSR across Arctic region to U.S., 1986, EOS, Trans. A.G.U., 68, 44, p1377

Figure Caption:

Figure 1: Map view of principal geographical features in Arctic.

Figure 2a: Hand digitized seismogram recorded by COP for event located at epicenter of 51.7 degree north in latitude and 176.1degree east in longitude.

Figure 2b: Group velocity dispersion curve for the seismogram shown in figure 1a.

Figure 3a: Map of grid divisions used in this study.

Figure 3b: Map of Rayleigh wave ray path coverage used in this study.

Figure 4a: Example of the resolution matrix plot of our stochastic inversion result.

Figure 4b: Example of the covariance matrix plot of our stochastic inversion result.

Figure 5a: Rayleigh wave group velocity contour plot of 19.9 second period from our stochastic inversion result.

Figure 5b: Rayleigh wave group velocity contour plot of 41.6 second period from our stochastic inversion result.

Figure 6: Resolution Kernel of our shear wave velocity starting model.

Figure 7: A series of cross-section maps of crustal structure from North American side to North Eurasia side. The numbers above each section are the grid division number which has been cut through by this section.

23

Figure 8: A series of cross-section maps of upper mantle structures from North American side to North Eurasia side. The numbers above each section are the grid division number which has been cut through by this section.

Figure 9: Cross section maps of upper mantle structures. One cut through grid 1, 4, 8, 13, 17 and 21, and the other cut through grid 2, 4, 8, 14, 18, 22 and 24.

Figure 10: Shear wave velocity profile in the vertical direction for grid 13.

Figure 11: Shear wave velocity profile in the vertical direction for grid 14 and 18.

Figure 12: Shear wave velocity profile in the vertical direction for grid 11 and 16.

Figure 13: Shear wave velocity profile in the vertical direction for grid 7 and 20.

Figure 14: Global surface wave ray map of 20 second period for our final model.

Figure 15: Synthetic seismograms for the source located at Novaya Zemlya and the WWSSN stations located in the United States for the initial model.

Figure 16: Synthetic seismograms for the source located at Novaya Zemlya and the WWSSN stations located in the United States for the improved model.

Figure 17: Observed seismograms for the source located at Novaya Zemlya and the WWSSN stations located in the United States.

24

TABLE 1

Station code	Latitude	Longitude
AKU	65 41 12.0 N	18 06 24.0 W
COL	64 54 00.0 N	147 47 36.0 W
COP	55 41 00.0 N	12 26 00.0 E
ESK	55 19 00.0 N	03 12 18.0 W
GDH	69 15 00.0 N	53 32 00.0 W
KBS	78 55 03.0 N	11 55 26.0 W
KEV	69 45 19.0 N	27 00 24.0 W
KON	59 38 56.7 N	09 35 53.6 E
KTG	70 25 00.0 N	21 59 00.0 W
NUR	60 30 32.4 N	24 39 05.1 E
UME	63 48 54.0 N	20 14 12.0 E

TABLE 2

Event	Data	Time	Depth	Mag.	Latitude	Longitude
01	06–05–70	10:31:54.30	33.0	5.5	63.37	146.23
02	01–27–79	18:57:55.00	17.0	6.0	54.77	−160.75
03	05–20–79	08:14:00.10	71.0	6.5	56.65	−155.27
04	09–01–79	05:27:17.60	69.0	6.4	53.98	−164.80
05	09–14–79	07:28:32.00	27.0	5.9	53.66	169.73
06	09–23–79	10:17:20.80	43.0	5.8	52.29	174.03
07	10–18–79	03:35:26.90	62.0	6.0	51.86	177.13
08	11–09–79	13:45:47.60	33.0	5.7	55.64	164.11
09	11–20–79	17:36:01.20	10.0	6.0	71.19	−07.97
10	03–22–80	10:27:40.10	69.0	5.7	55.71	161.48
11	11–04–80	20:26:00.70	33.0	6.1	53.82	160.74
12	11–21–80	14:56:13.40	53.0	6.0	51.80	−175.86
13	12–14–80	06:27:29.80	24.0	5.6	52.99	171.06
14	02–09–81	12:47:59.00	33.0	5.5	54.97	165.99
15	05–25–81	04:59:57.20	00.0	5.5	68.21	53.66
16	11–08–81	21:56:10.83	33.0	5.6	61.81	153.67
17	05–31–82	10:21:15.00	33.0	6.4	55.14	165.40
18	06–04–82	03:01:04.10	59.0	5.8	51.60	−176.67
19	07–31–82	06:29:15.50	38.0	6.2	51.76	176.14
20	09–12–82	16:50:37.70	33.0	5.5	52.82	−166.95
21	11–21–82	23:27:11.50	35.0	6.2	55.40	163.18
22	02–14–83	08:10:03.60	33.0	6.0	54.97	−158.76
23	04–03–83	19:14:05.00	116.0	5.6	51.98	179.26
24	06–10–83	02:13:22.90	10.0	5.6	75.53	122.76
25	06–28–83	03:25:17.07	18.5	6.0	60.22	−141.29
26	07–12–83	15:10:03.40	37.0	6.1	61.03	−147.29
27	09–07–83	19:22:05.10	45.0	6.2	60.98	−146.50
28	12–27–83	23:05:57.90	53.0	6.1	54.19	−163.86
29	08–14–84	01:02:08.40	20.0	5.7	61.86	−148.90
30	11–19–84	12:06:37.30	58.0	5.6	51.78	−174.73
31	03–09–85	14:08:04.38	11.8	5.9	66.24	−150.03
32	09–10–85	01:26:04.42	16.6	5.7	60.39	168.31
33	10–05–85	15:24:02.27	10.0	6.5	62.24	−124.27

TABLE 3

Path	Event	Station	Distance	Path	Event	Station	Distance
01	01	UME	5211.56	38	11	NUR	6745.15
02	01	NUR	5413.73	39	12	COP	8065.71
03	02	ESK	7630.21	40	12	KBS	5459.77
04	02	GDH	5055.69	41	12	NUR	7418.73
05	02	KBS	5025.31	42	17	AKU	6600.48
06	02	KTG	5733.85	43	17	KON	7096.85
07	03	KBS	4765.36	44	18	COP	8082.99
08	03	KTG	5430.03	45	18	KEV	6321.23
09	03	GDH	4703.26	46	18	KON	7657.96
10	03	NUR	7012.89	47	18	UME	7122.46
11	05	GDH	5926.19	48	19	COP	8000.80
12	05	KBS	5291.77	49	19	KBS	5493.92
13	05	KEV	6248.05	50	19	KEV	6396.37
14	05	KTG	6209.05	51	19	KON	7594.14
15	05	NUR	6972.61	52	19	NUR	7299.93
16	05	UME	6713.54	53	22	KEV	5636.59
17	06	COP	7916.39	54	22	NUR	7196.17
18	06	KBS	5438.69	55	23	COL	3180.30
19	06	KEV	6359.71	56	23	COP	7599.88
20	06	NUR	7203.68	57	23	NUR	6812.58
21	07	KEV	6373.66	58	23	KBS	5362.75
22	07	NUR	7306.13	59	23	KEV	6384.26
23	07	UME	7021.38	60	24	GDH	3930.67
24	08	UME	6398.93	61	24	KON	4263.31
25	09	KON	1511.03	62	24	NUR	3835.72
26	09	ESK	1784.35	63	25	GDH	3913.63
27	09	NUR	1867.69	64	25	KBS	4208.50
28	10	COP	7341.49	65	25	KEV	4683.42
29	10	GDH	5856.45	66	25	KON	6474.45
30	10	KBS	5057.53	67	25	NUR	6560.37
31	10	KEV	6069.82	68	26	AKU	5339.04
32	10	KTG	6010.09	69	26	COP	6940.29
33	10	NUR	6570.46	70	27	KEV	4763.68
34	11	COL	3069.20	71	27	KON	6481.90
35	11	COP	7525.62	72	28	KBS	5115.86
36	11	KBS	5266.27	73	29	KBS	4125.96
37	11	KEV	6282.69	74	31	COP	6401.60

TABLE 4

Grid #	1	2	3	4	5	6	7	8
Error	0.111	0.093	0.083	0.085	0.117	0.137	0.123	0.112
Grid #	9	10	11	12	13	14	15	16
Error	0.104	0.095	0.095	0.107	0.132	0.097	0.105	0.080
Grid #	17	18	19	20	21	22	23	24
Error	0.093	0.098	0.089	0.093	0.127	0.114	0.078	0.091

Fig. 1

29

Fig. 2a

Displacement

Time (Sec)

30

Fig. 2b

31
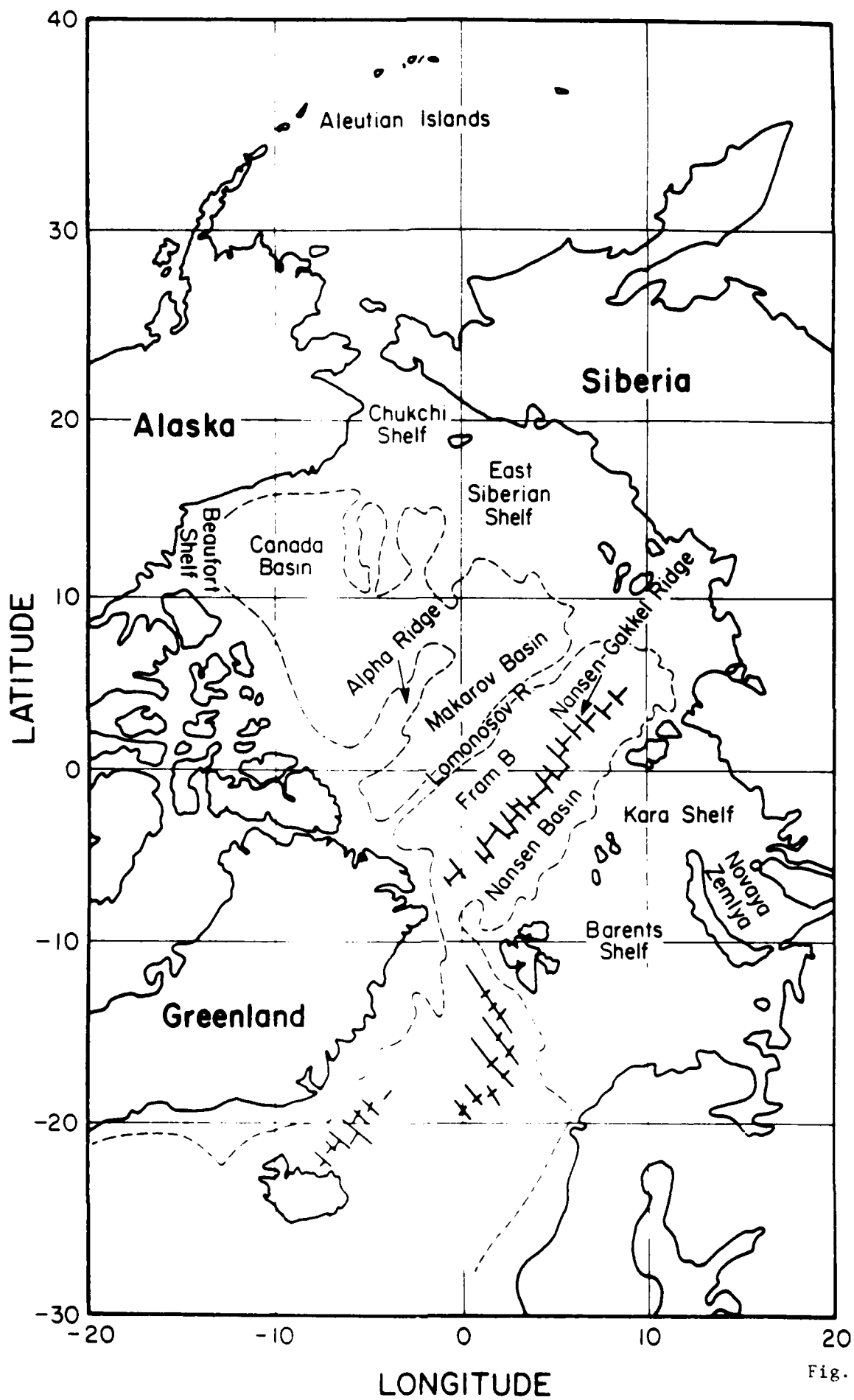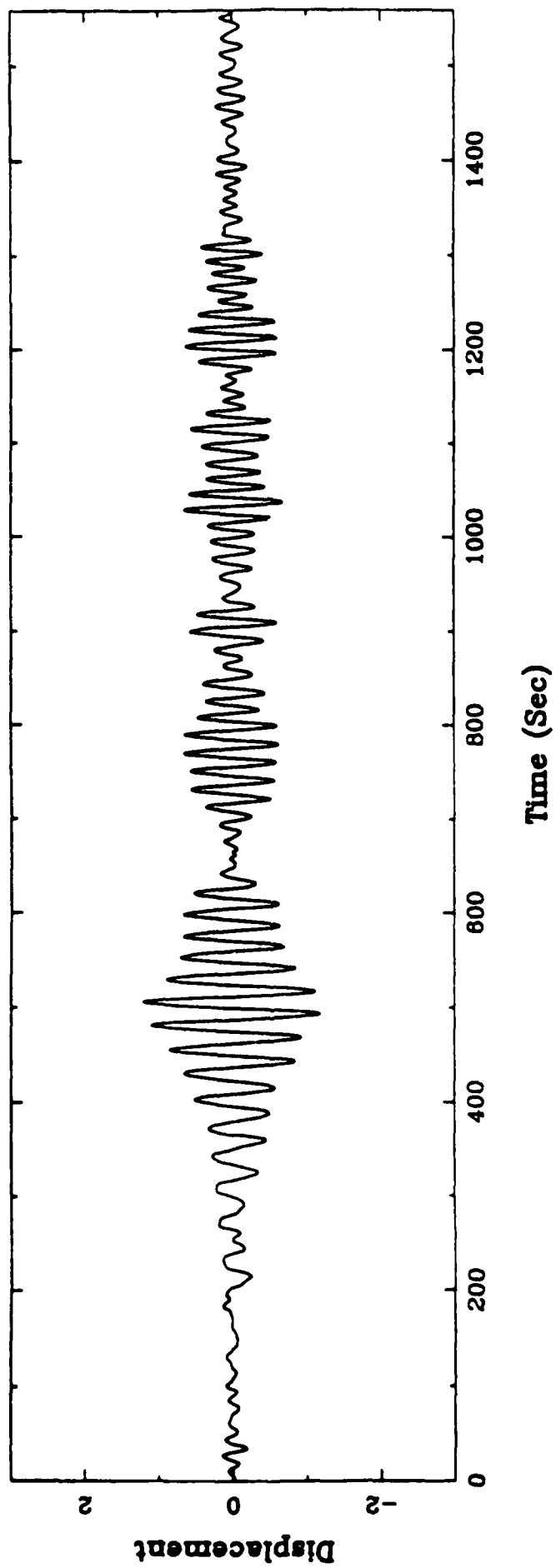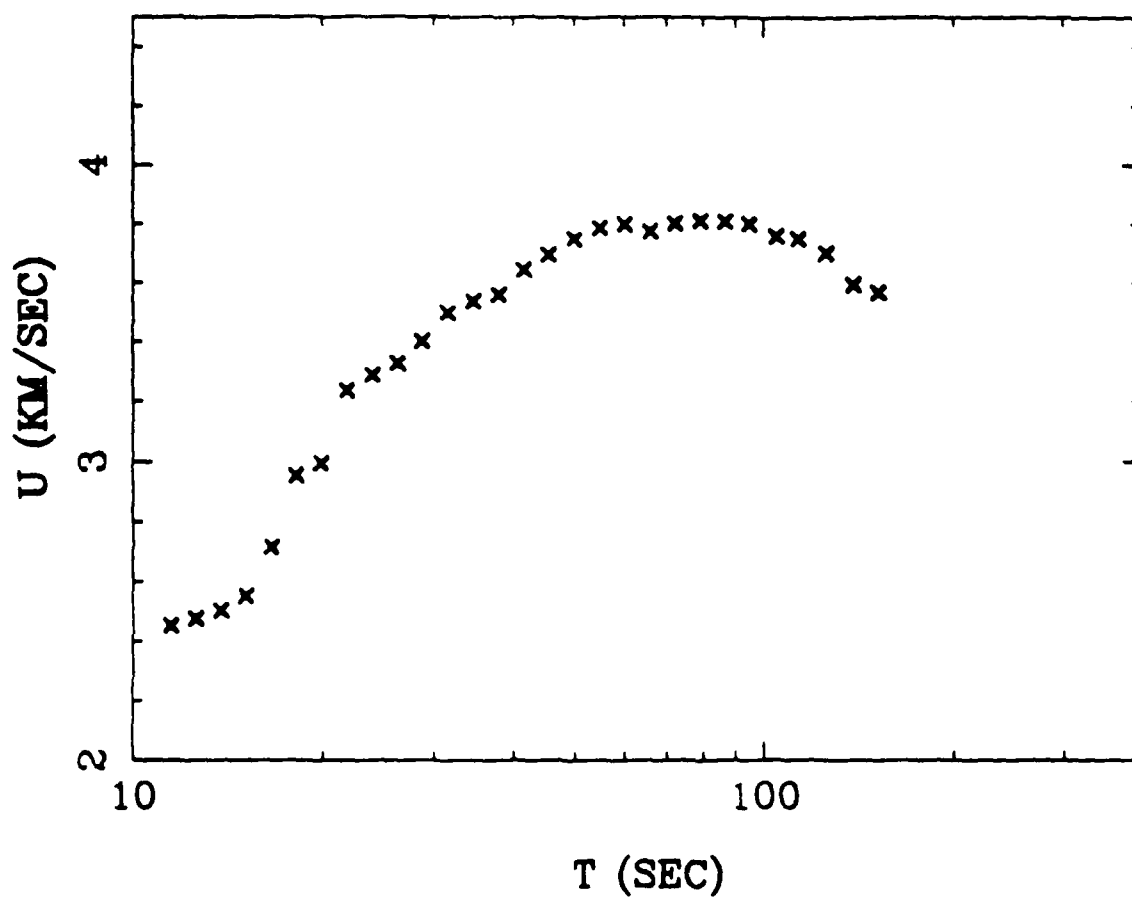
Rotated World Map with Pole at (0.0,0.0)
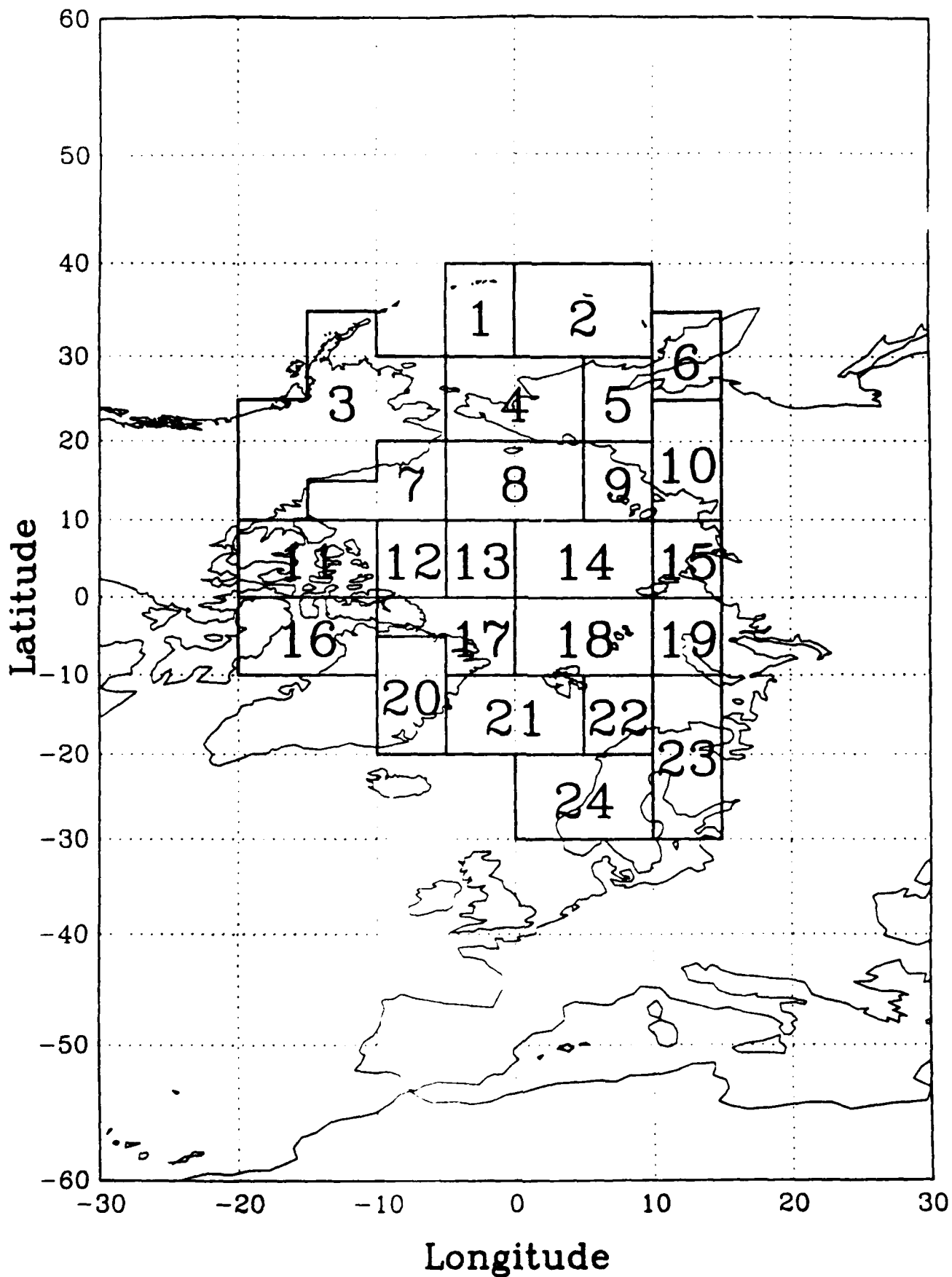
Fig. 3a

Rotated World Map with Pole at (0.0,0.0)
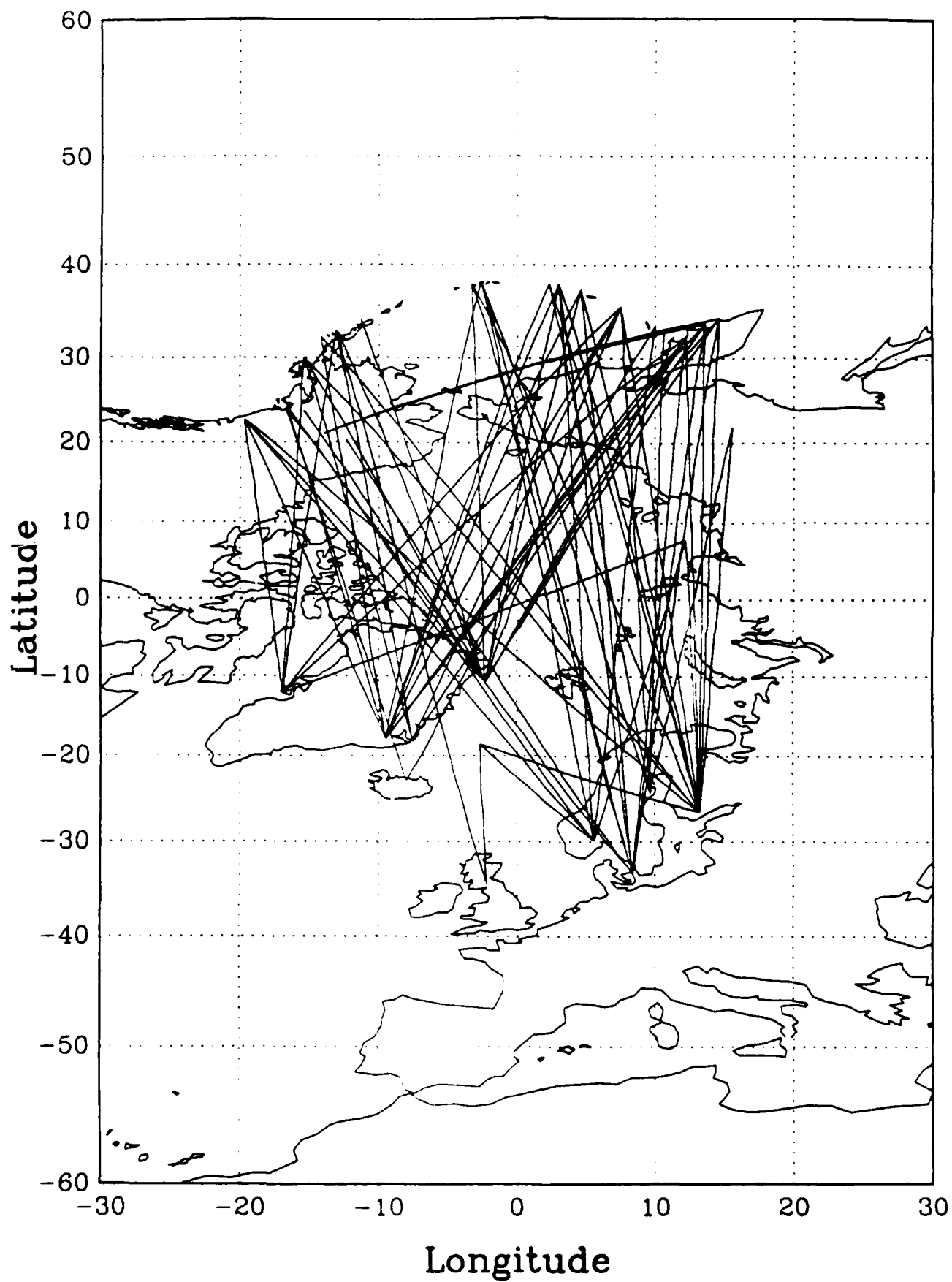
Fig. 3b

RESOLUTION MATRIX (T=41.6)
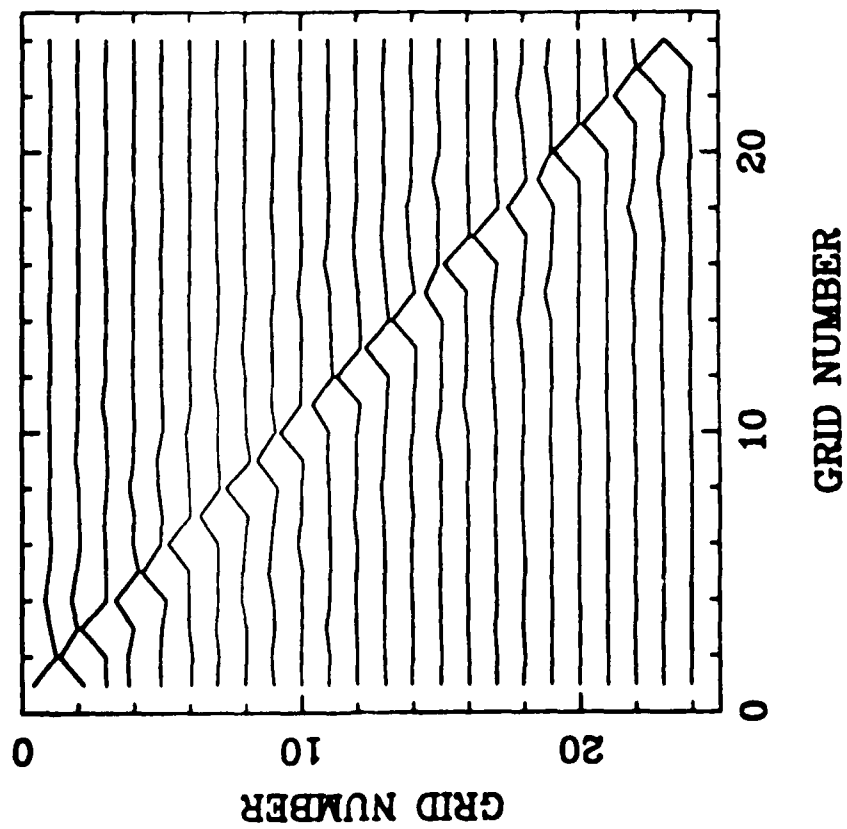
COVARRANCE MATRIX (T=41.6)

GRID NUMBER

GRID NUMBER

Fig. 4a

Fig. 4b

34
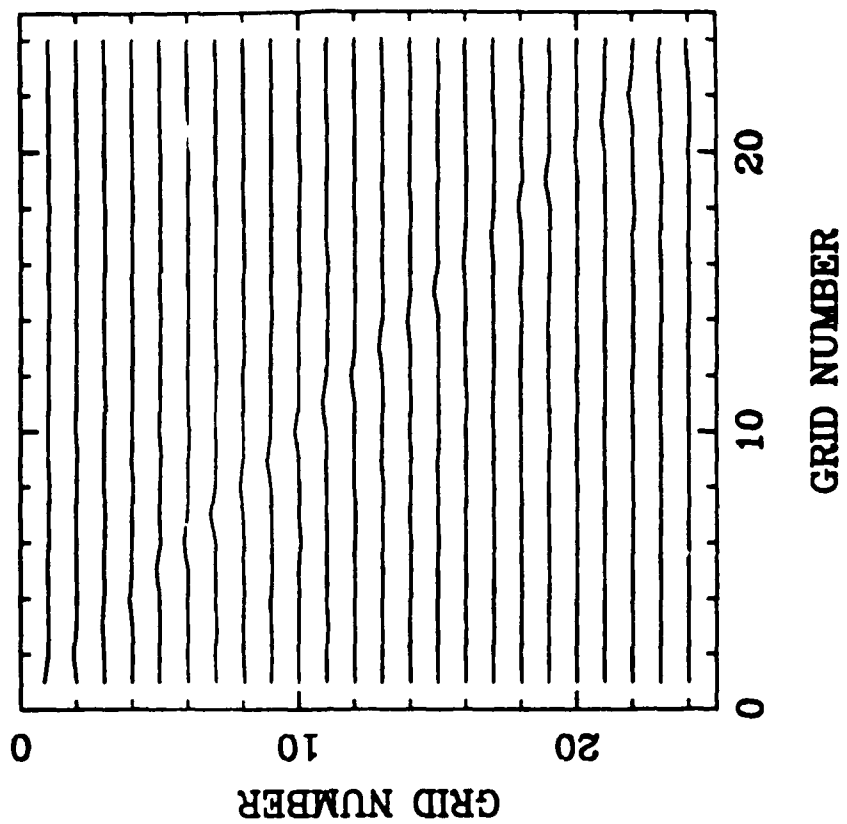
VELOCITY CONTOUR PLOT (T = 19.9)
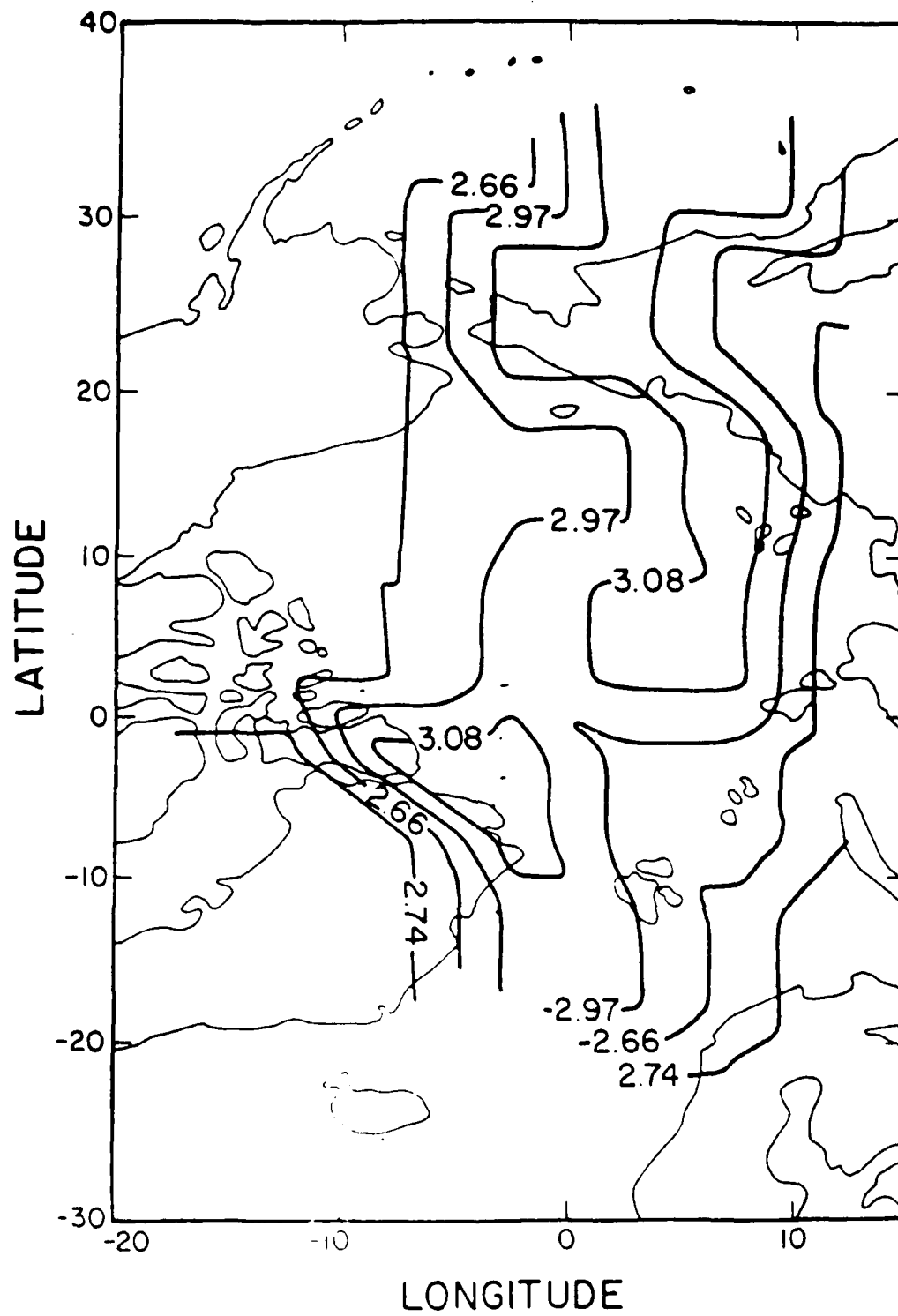
Fig. 5a

VELOCITY CONTOUR PLOT (T = 41.6)
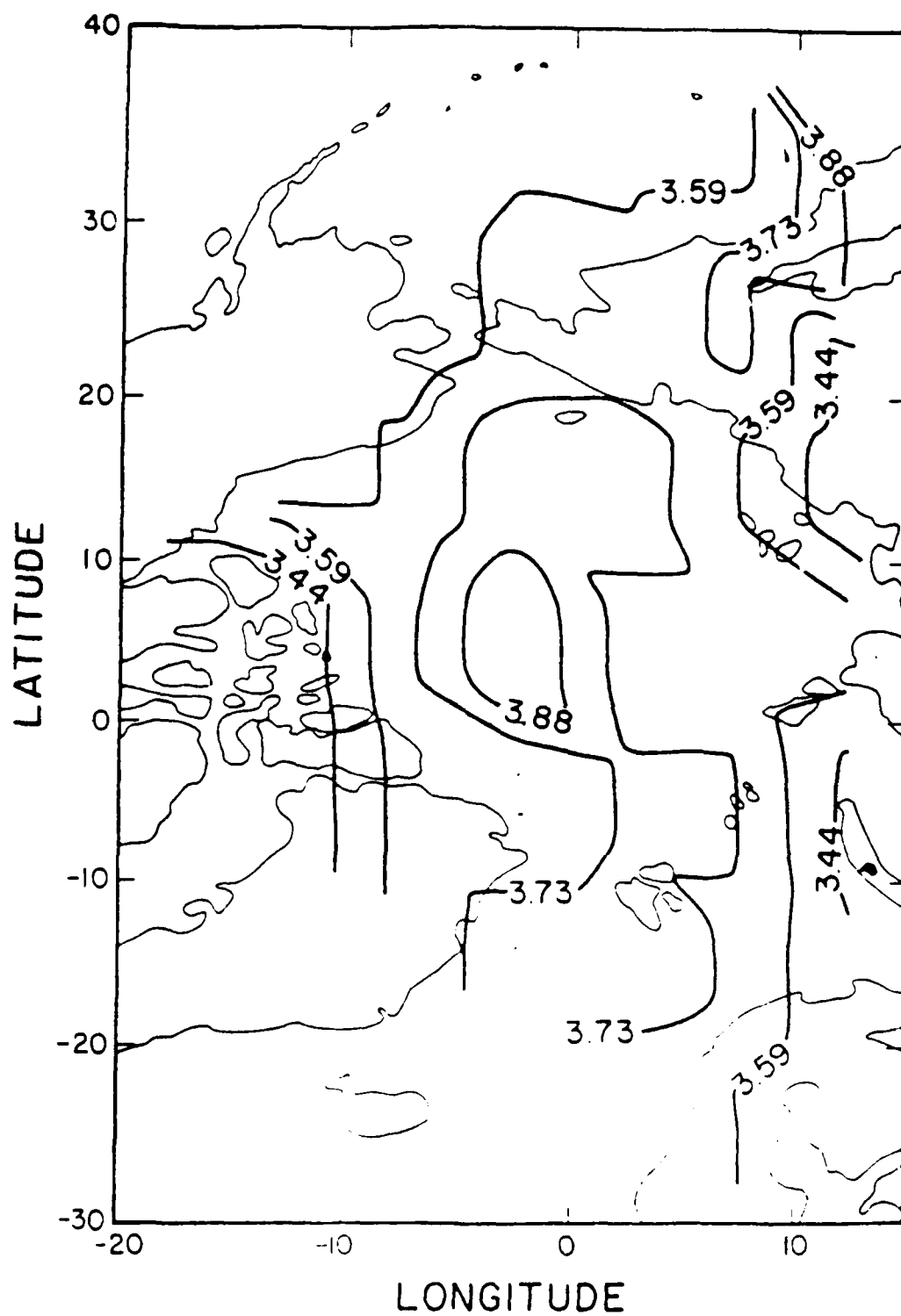
Resolving Kernels at Different Depths
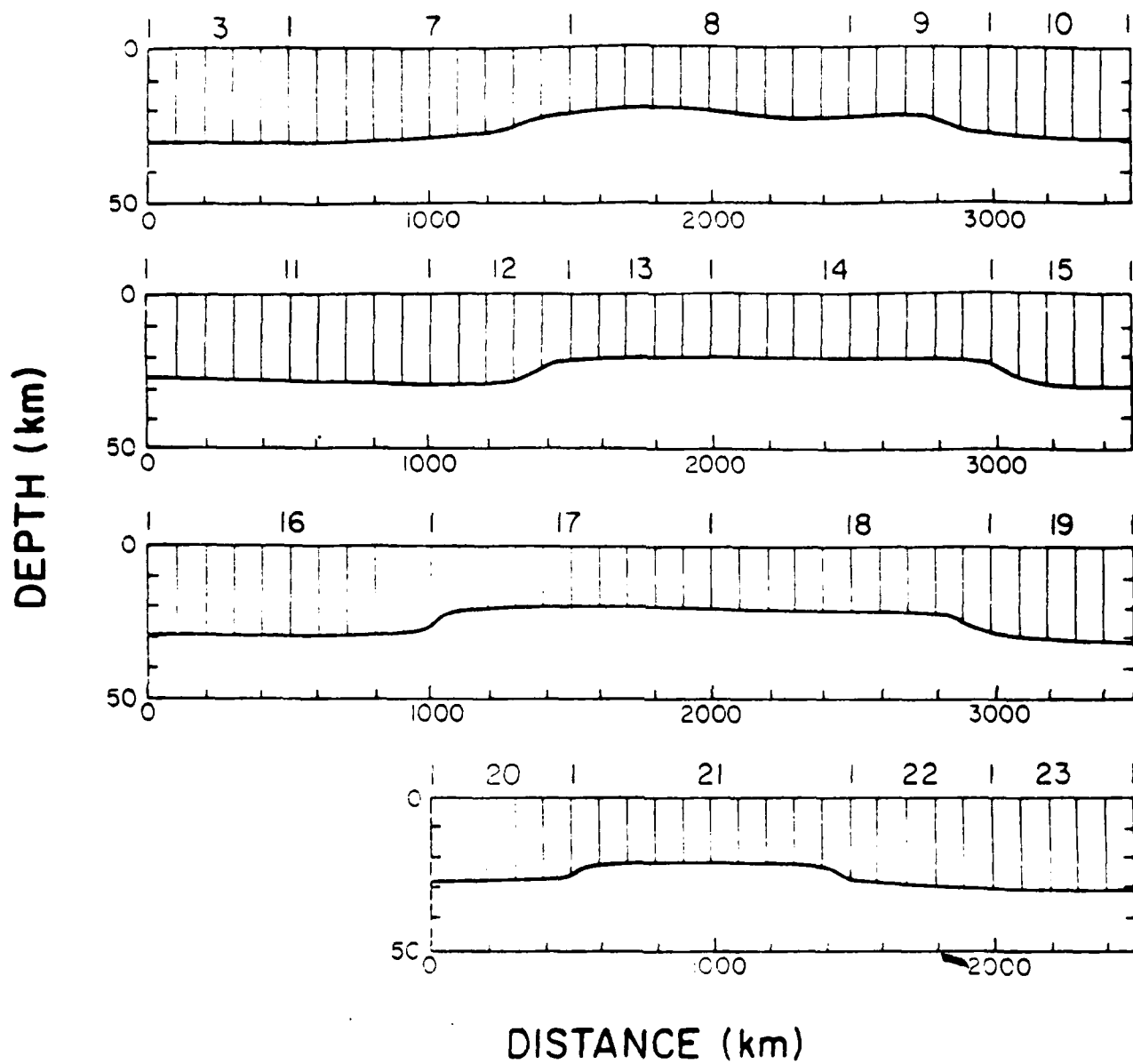
1.5

6.5

15.0

25.0

37.5

57.5

82.5

110.0

140.0

177.5

225.0

275.0

350.0

0   200   400

Depth (km)

Resolving Kernels

Fig. 6

Fig. 7
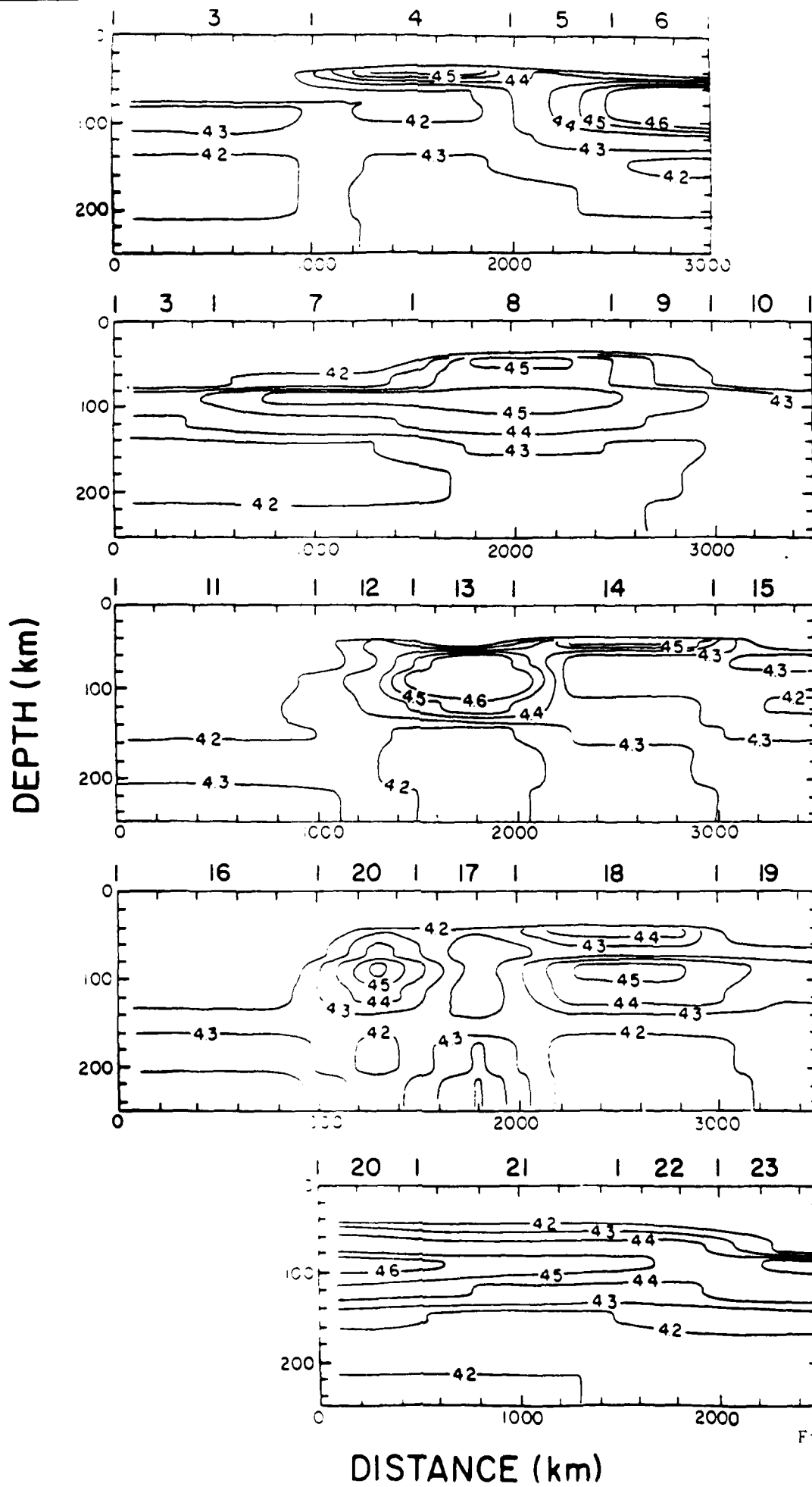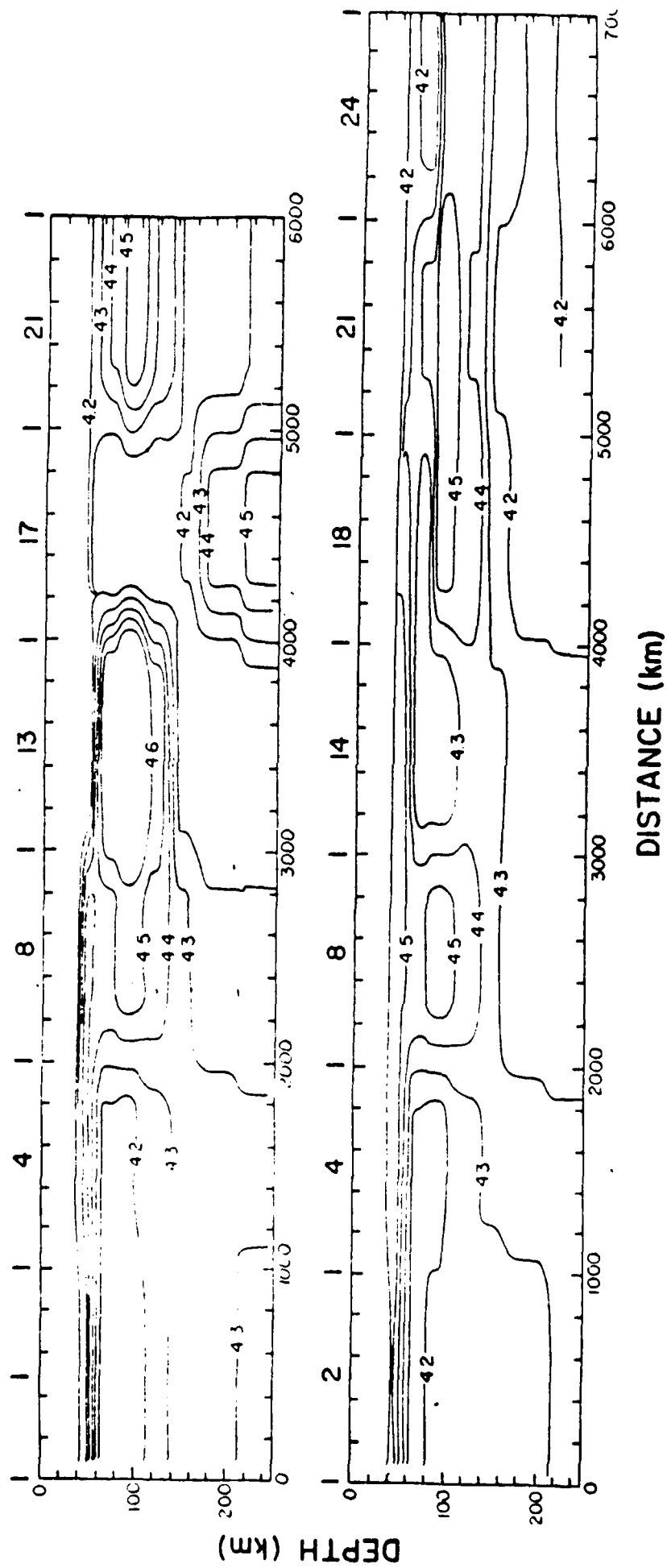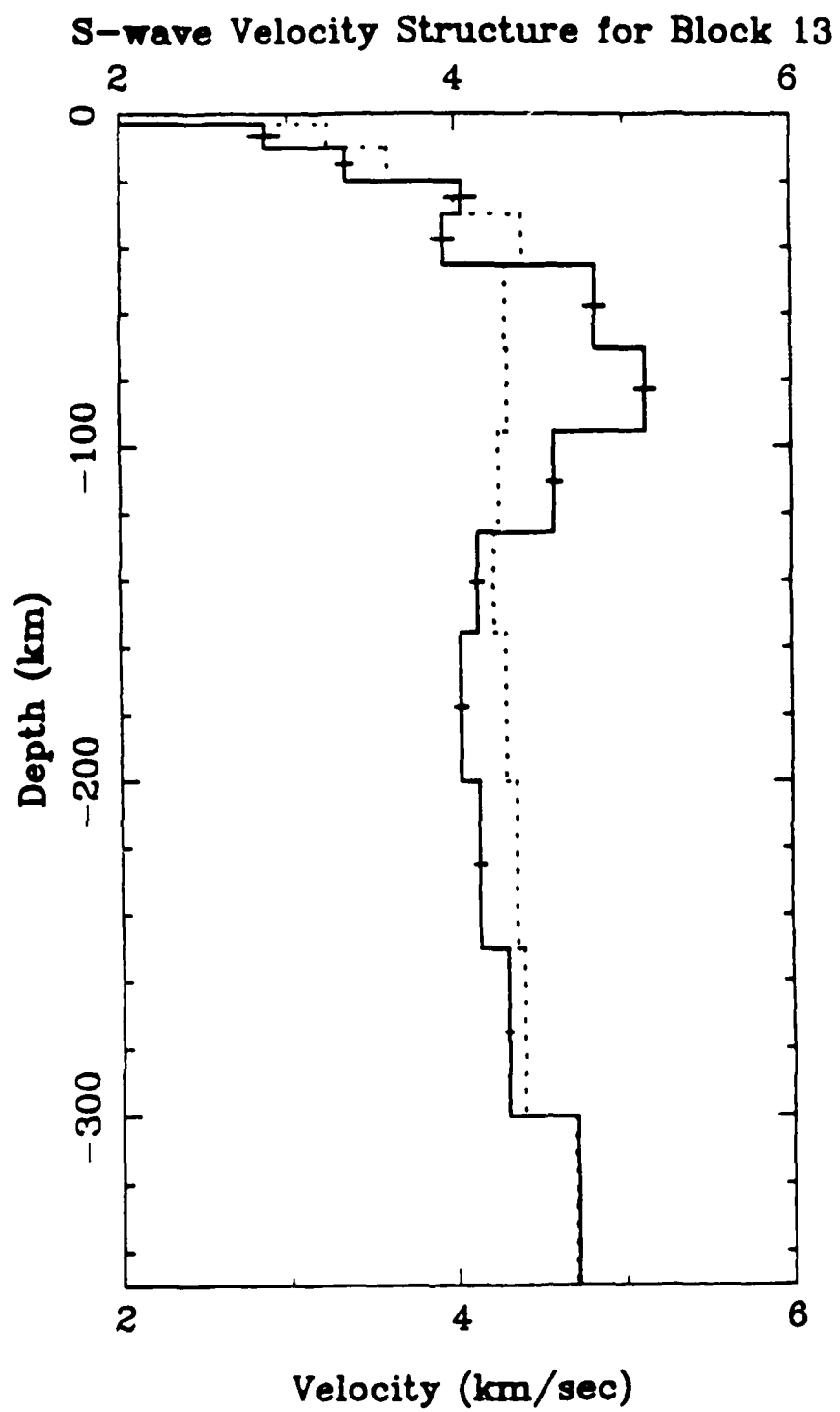
38

Fig. 8

DEPTH (km)

DISTANCE (km)

39

Fig. 9

S-wave Velocity Structure for Block 13

Fig. 10

41
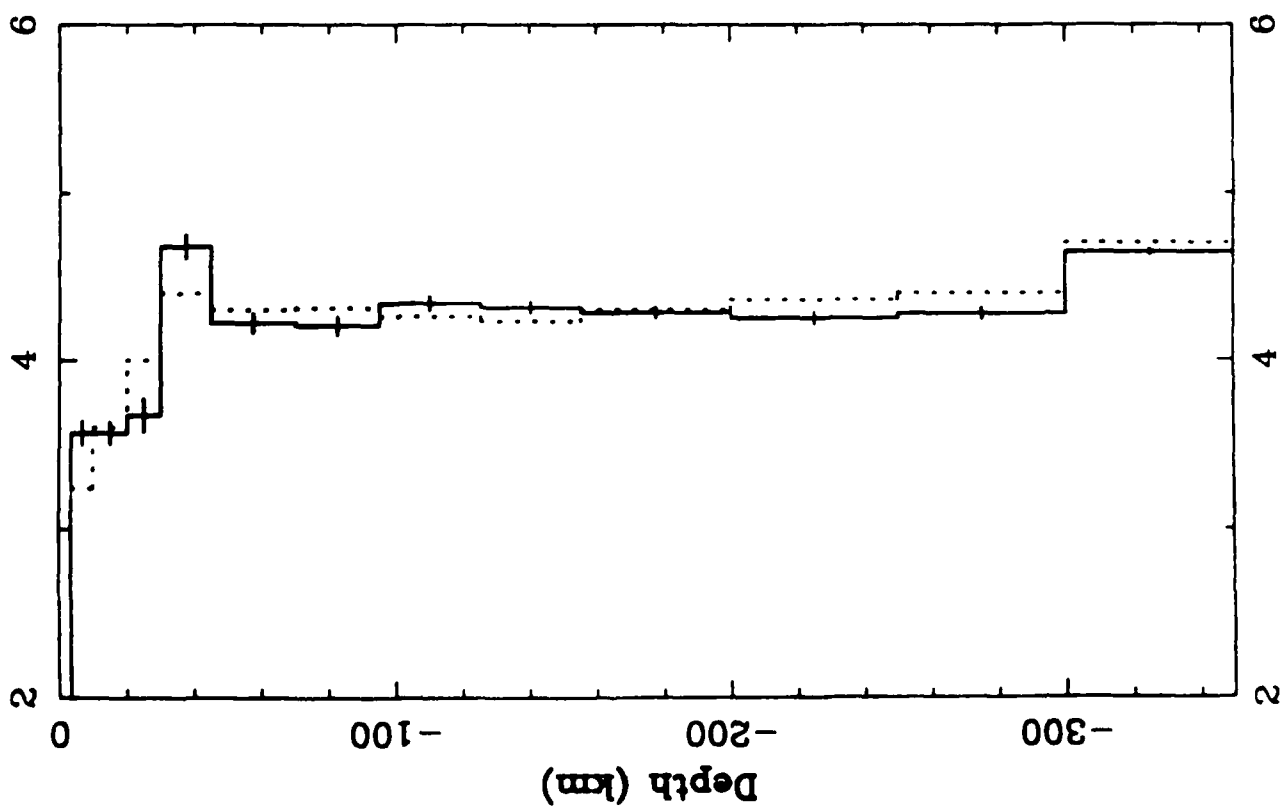
Fig. 11b

Fig. 11a

Fig. 12a

S-wave Velocity Structure for Block 11
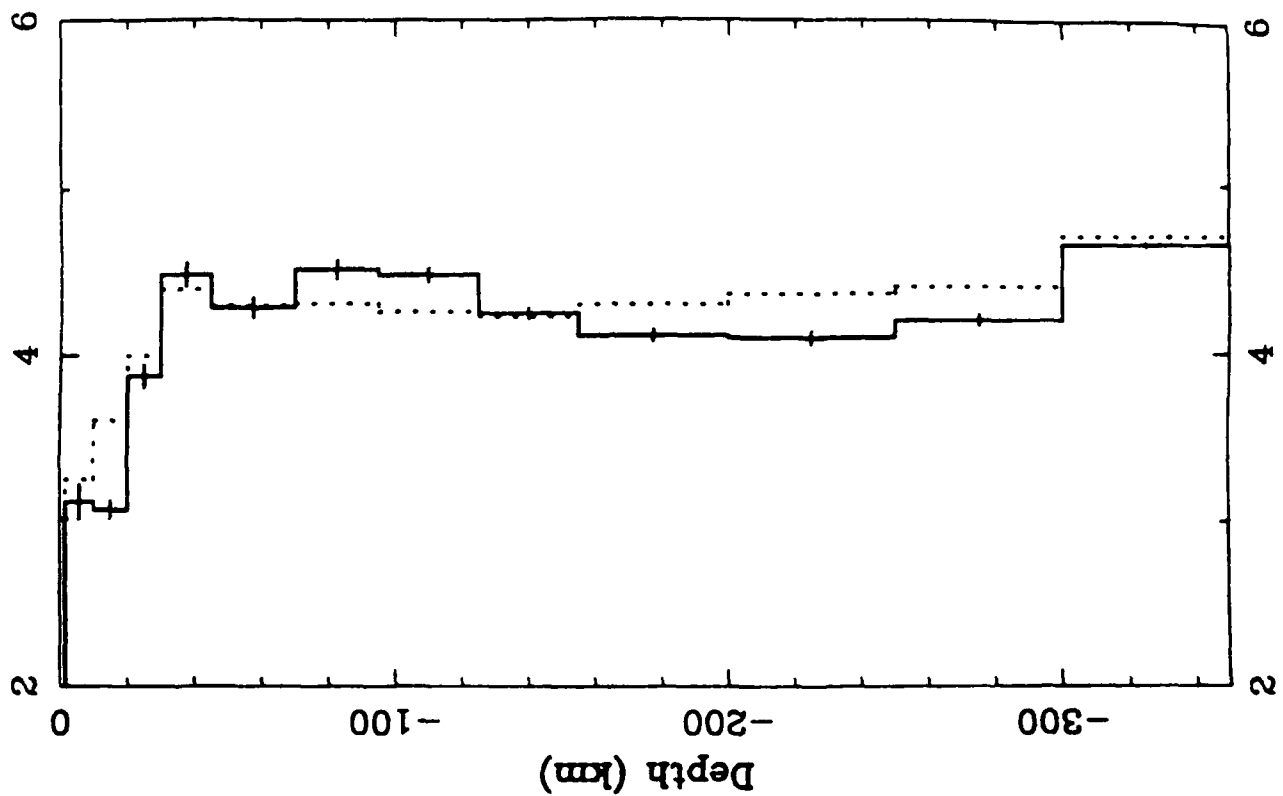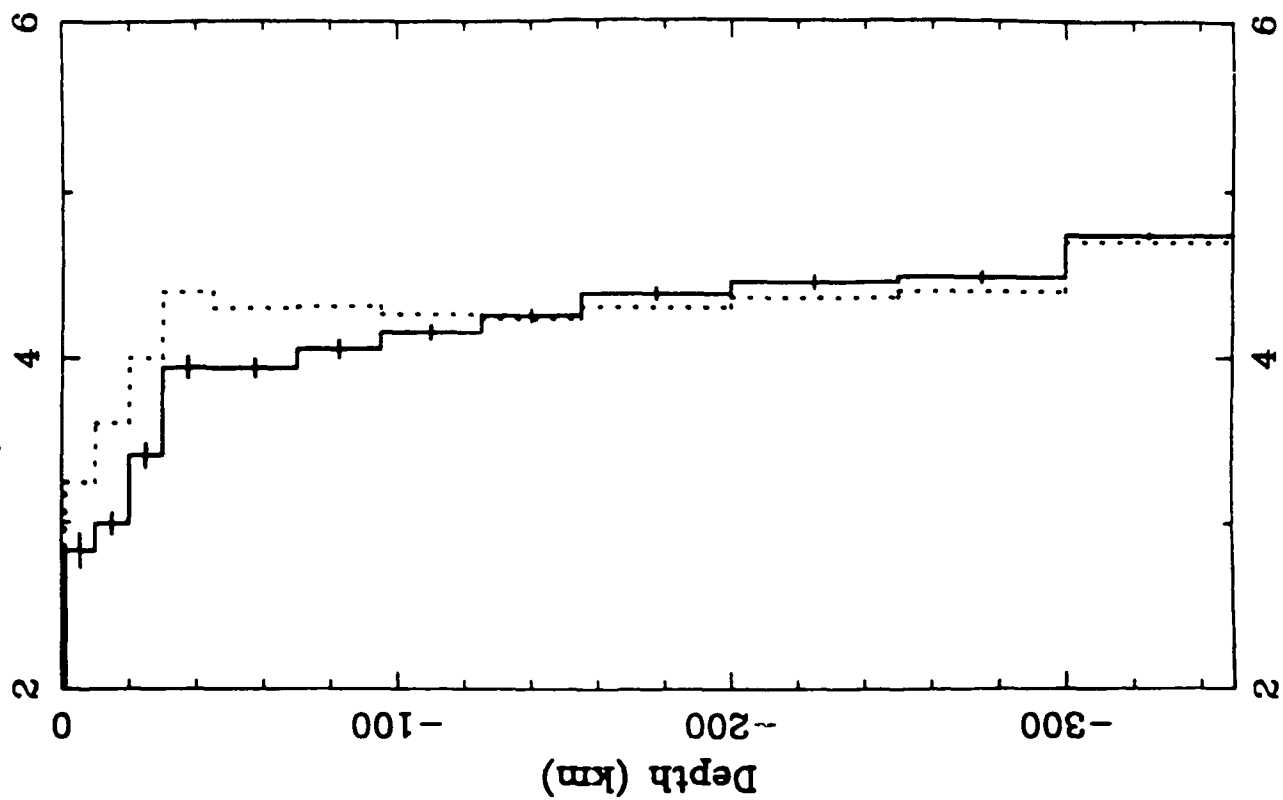
Fig. 12b

S-wave Velocity Structure for Block 16

43

Fig. 13b

Fig. 13a

44
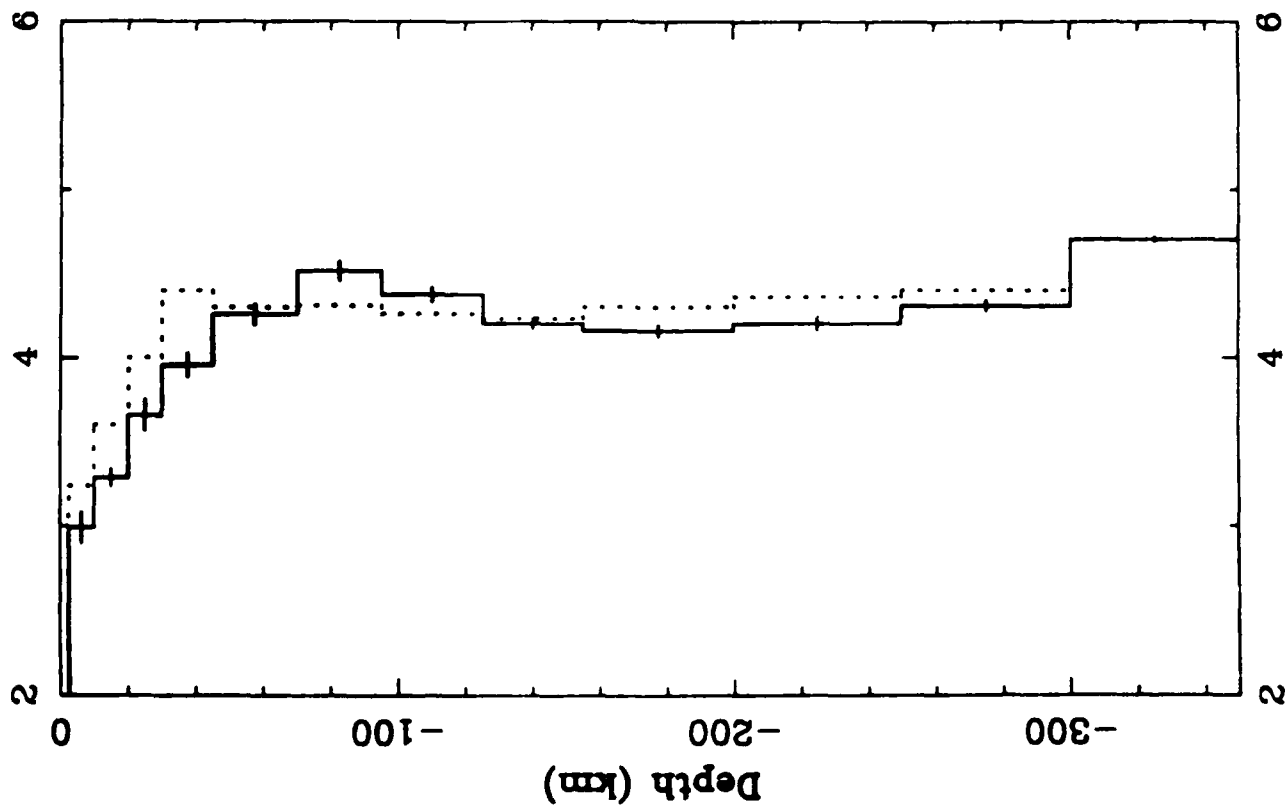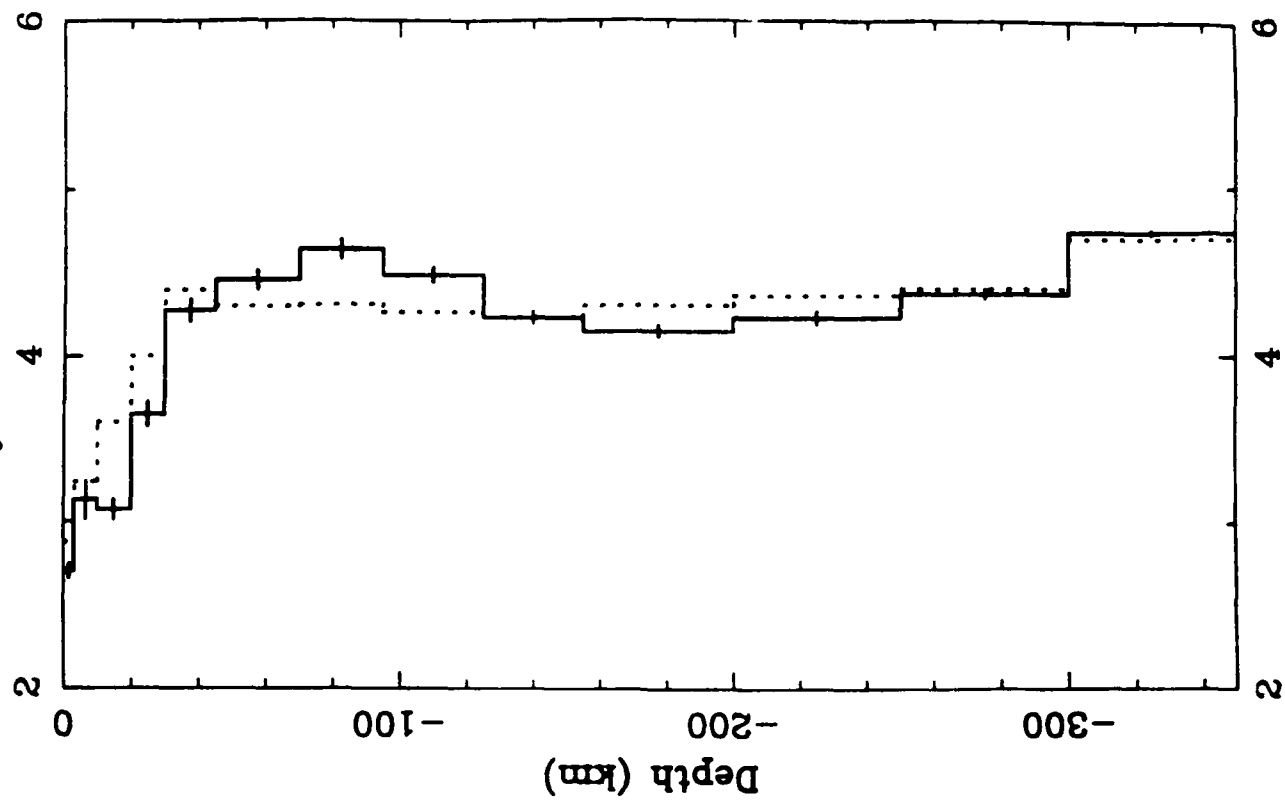
Novaya Zemlya T = 20 Seconds

Latitude

Longitude

Fig. 14

Novaya Zemlya ($\phi = 55.0^0$ $\lambda = 73.0^0$)

($T = 20$ Seconds, $L_0 = 1.0$, $S_0 = 1.0$, $\delta_1 = 2^0$, $Q = 500$)

(Peak Amplitude = 0.85E-02)

Station Number

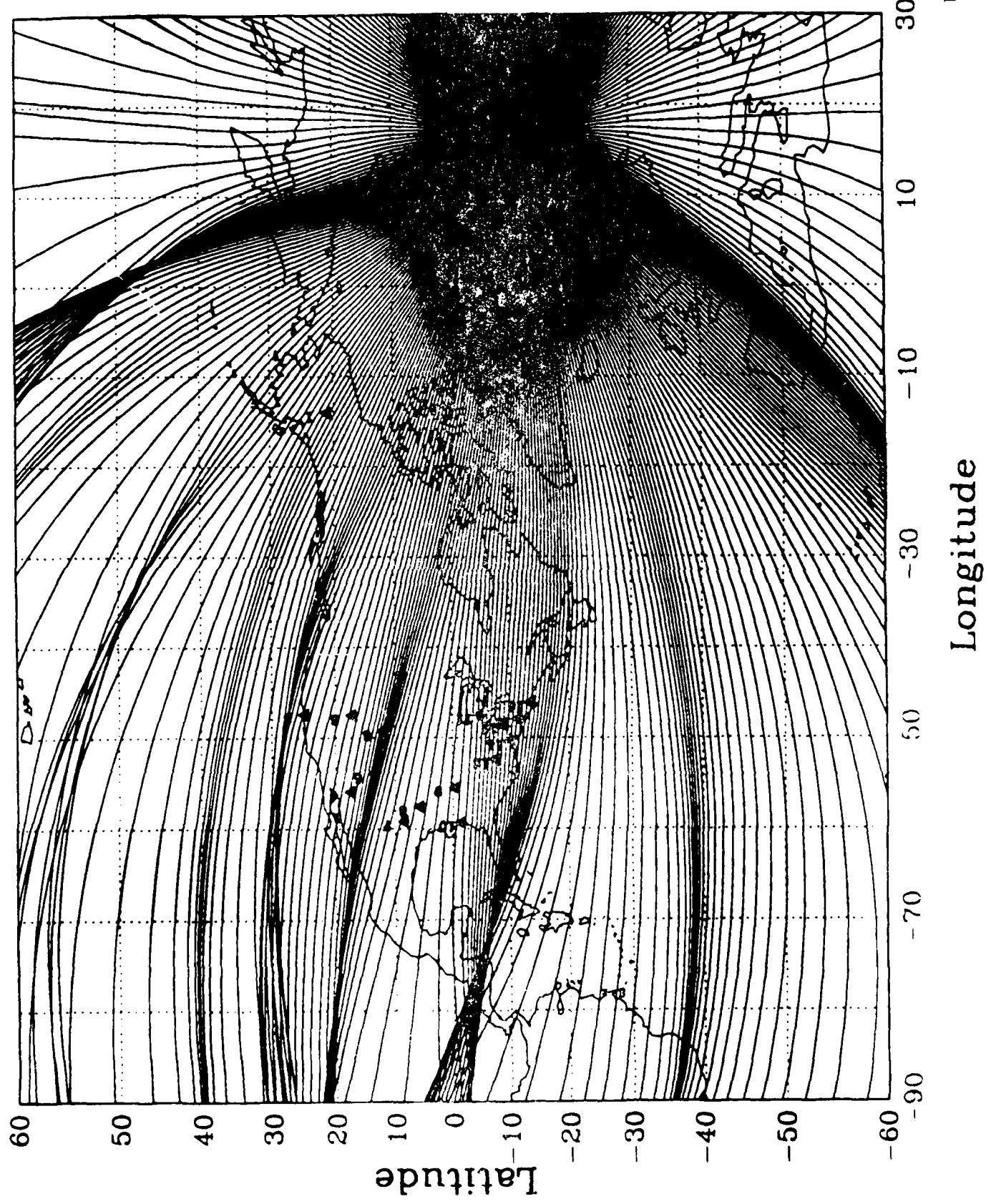Time(Seconds)
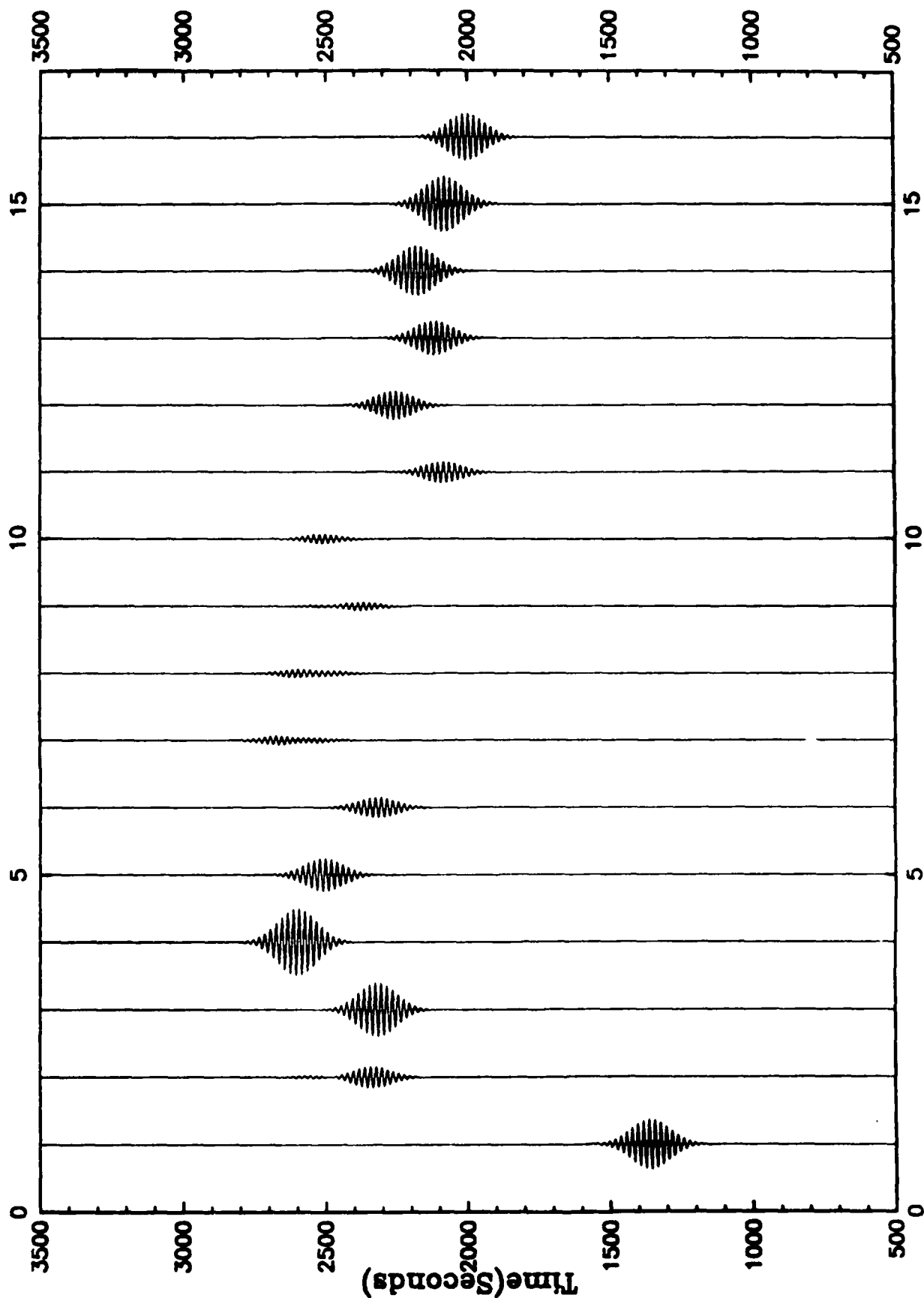
Fig. 15

46

Novaya Zemlya ($\phi = 55.0^0$ $\lambda = 73.0^0$)
($T = 20$ Seconds, $L_0 = 1.0$, $S_0 = 1.0$, $\delta_1 = 2^0$, $Q = 500$)

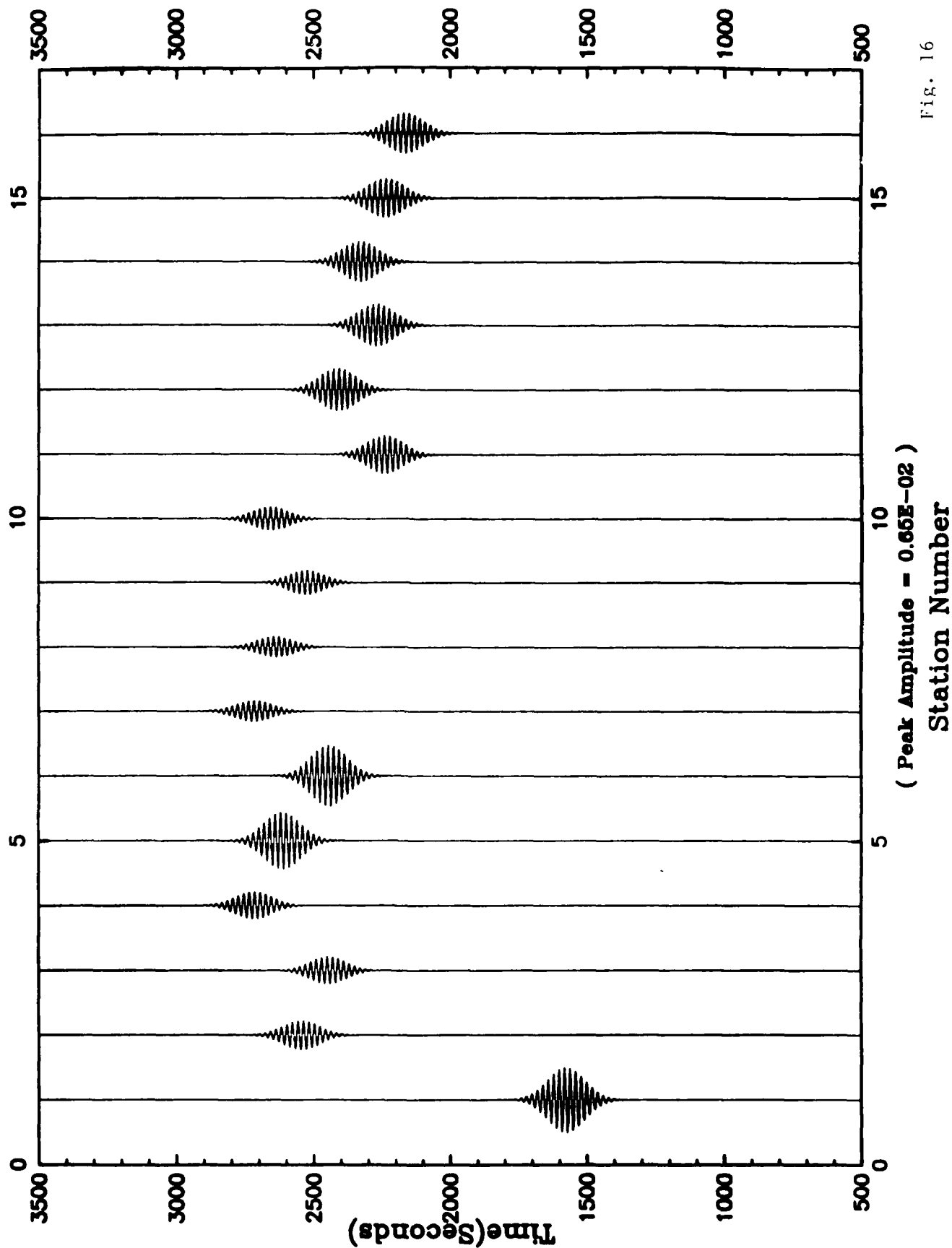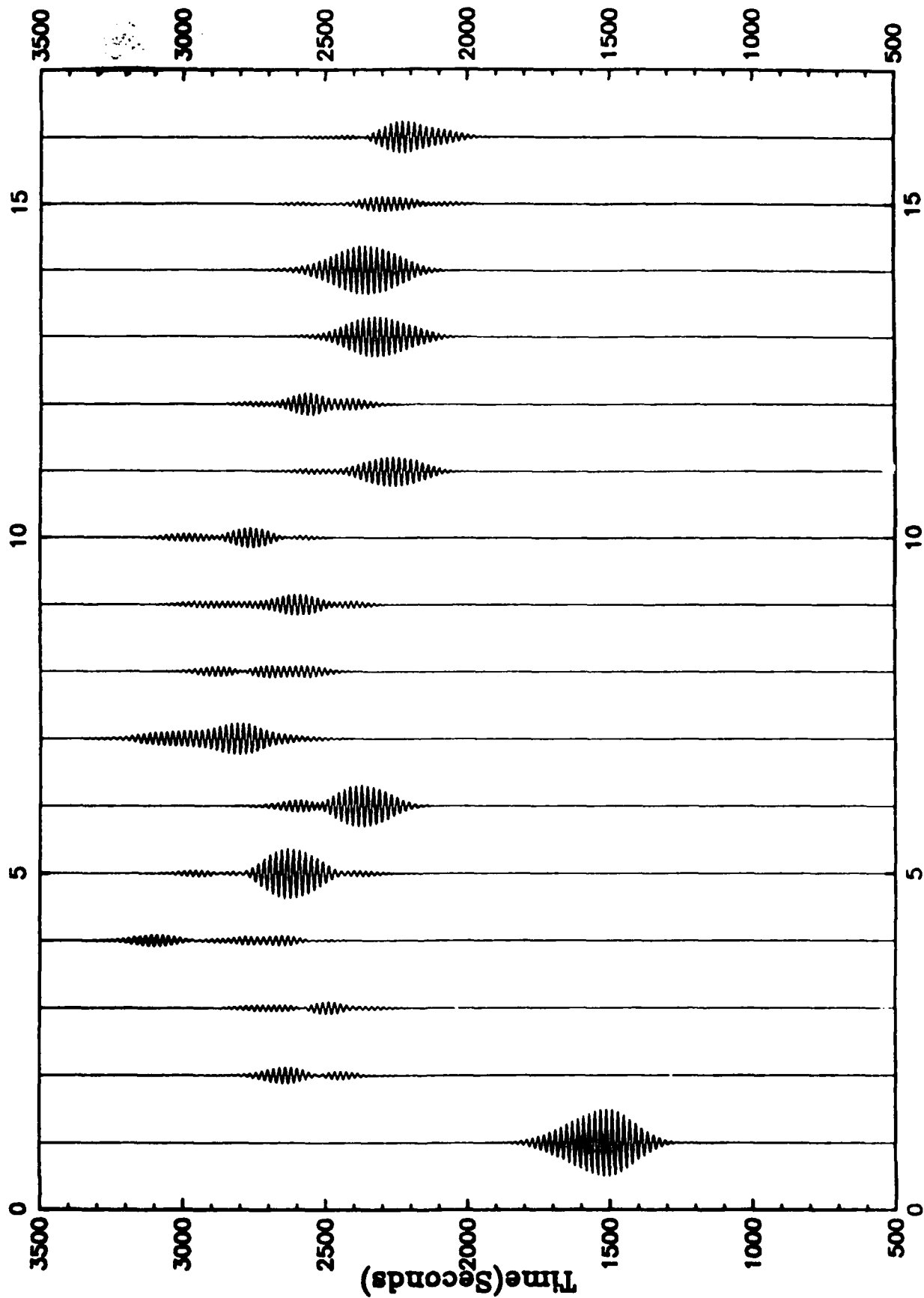(Peak Amplitude = 0.65E-02)
Station Number

Time(Seconds)

Fig. 16

47

Novaya Zemlya ($\phi = 55.0^0$ $\lambda = 73.0^0$)
($T = 20$ Seconds, $\Gamma_0 = 30.0$)

(Observational seismograms)
Station Number

Time(Seconds)

Fig. 17

48

Professor Keiiti Aki
Center for Earth Sciences
University of Southern California
University Park
Los Angeles, CA 90089-0741

Professor Charles B. Archambeau
Cooperative Institute for Resch
  in Environmental Sciences
University of Colorado
Boulder, CO 80309

Dr. Thomas C. Bache Jr.
Science Applications Int'l Corp.
10210 Campus Point Drive
San Diego, CA 92121   (2 copies)

Dr. Muawia Barazangi
Institute for the Study of the
  Continent
SNEE Hall
Cornell University
Ithaca, NY 14853

Dr. Douglas R. Baumgardt
Signal Analysis & Systems Div.
ENSCO, Inc.
5400 Port Royal Road
Springfield, VA 22151-2388

Dr. Jonathan Berger
Institute of Geophysics and
  Planetary Physics
Scripps Institution of Oceanography
A-025
University of California, San Diego
La Jolla, CA 92093

Dr. S. Bratt
Science Applications Int'l Corp.
10210 Campus Point Drive
San Diego, CA 92121

Dr. Lawrence J. Burdick
Woodward-Clyde Consultants
P.O. Box 93245
Pasadena, CA 91109-3245 (2 copies)

Professor Robert W. Clayton
Seismological Laboratory/Div. of
  Geological & Planetary Sciences
California Institute of Technology
Pasadena, CA 91125

Dr Karl Coyner
N. E. Research, Inc.
76 Olcott Drive
White River Junction, VT 05001

Dr. Steven Day
Dept. of Geological Sciences
San Diego State U.
San Diego, CA 92182

Dr. Zoltan A. Der
ENSCO, Inc.
5400 Port Royal Road
Springfield, VA 22151-2388

Professor John Ferguson
Center for Lithospheric Studies
The University of Texas at Dallas
P.O. Box 830688
Richardson, TX 75083-0688

Professor Stanley Flatte'
Applied Sciences Building
University of California,
Santa Cruz, CA 95064

Dr. Alexander Florence
SRI International
333 Ravenswood Avenue
Menlo Park, CA 94025-3493

Prof. Stephen Grand
University of Texas at Austin
Dept of Geological Sciences
Austin, TX 78713-7909

Dr. Henry L. Gray
Associate Dean of Dedman College
Department of Statistical Sciences
Southern Methodist University
Dallas, TX 75275

Professor Roy Greenfield
Geosciences Department
403 Deike Building
The Pennsylvania State University
University Park, PA 16802

Professor David G. Harkrider
Seismological Laboratory
Div of Geological & Planetary Sciences
California Institute of Technology
Pasadena, CA 91125

Dr. Vernon F. Cormier
Department of Geology & Geophysics
U-45, Room 207
The University of Conneticut
Storrs, Connecticut 06268

Professor Eugene Herrin
Institute for the Study of Earth
  and Man/Geophysical Laboratory
Southern Methodist University
Dallas, TX 75275

Professor Robert B. Herrmann
Department of Earth & Atmospheric
      Sciences
Saint Louis University
Saint Louis, MO 63156

Professor Bryan Isacks
Cornell University
Dept of Geological Sciences
SNEE Hall
Ithaca, NY 14850

Professor Lane R. Johnson
Seismographic Station
University of California
Berkeley, CA 94720

Professor Thomas H. Jordan
Department of Earth, Atmospheric
 and Planetary Sciences
Mass Institute of Technology
Cambridge, MA 02139

Dr. Alan Kafka
Department of Geology &
  Geophysics
Boston College
Chestnut Hill, MA 02167

Professor Leon Knopoff
University of California
Institute of Geophysics
  & Planetary Physics
Los Angeles, CA 90024

Professor Charles A. Langston
Geosciences Department
403 Deike Building
The Pennsylvania State University
University Park, PA 16802

Professor Donald V. Helmberger
Seismological Laboratory
Div of Geological & Planetary Sciences
California Institute of Technology
Pasadena, CA 91125

Dr. Gary McCartor
Mission Research Corp.
735 State Street
P.O. Drawer 719
Santa Barbara, CA 93102   (2 copies)

Professor Thomas V. McEvilly
Seismographic Station
University of California
Berkeley, CA 94720

Dr. Keith L. McLaughlin
S-CUBED,
A Division of Maxwell Laboratory
P.O. Box 1620
La Jolla, CA 92038-1620

Professor William Menke
Lamont-Doherty Geological Observatory
  of Columbia University
Palisades, NY 10964

Professor Brian J. Mitchell
Department of Earth & Atmospheric
  Sciences
Saint Louis University
Saint Louis, MO 63156

Mr. Jack Murphy
S-CUBED
A Division of Maxwell Laboratory
11800 Sunrise Valley Drive
Suite 1212
Reston, VA 22091 (2 copies)

Professor J. A. Orcutt
Institute of Geophysics and Planetary
  Physics, A-205
Scripps Institute of Oceanography
Univ. of California, San Diego
La Jolla, CA 92093

Professor Keith Priestley
University of Nevada
Mackay School of Mines
Reno, NV 89557

Professor Thorne Lay
Department of Geological Sciences
1006 C.C. Little Building
University of Michigan
Ann Arbor, MI 48109-1063

Dr. Randolph Martin III
New England Research, Inc.
76 Olcott Drive
White River Junction, VT 05001

Dr. Alan S. Ryall, Jr.
Center of Seismic Studies
1300 North 17th Street
Suite 1450
Arlington, VA 22209-2308   (4 copies)

Professor Charles G. Sammis
Center for Earth Sciences
University of Southern California
University Park
Los Angeles, CA 90089-0741

Professor Christopher H. Scholz
Geological Sciences
Lamont-Doherty Geological Observatory
Palisades, NY 10964

Dr. Jeffrey L. Stevens
S-CUBED,
A Division of Maxwell Laboratory
P.O. Box 1620
La Jolla, CA 92038-1620

Professor Brian Stump
Institute for the Study of Earth & Man
Geophysical Laboratory
Southern Methodist University
Dallas, TX 75275

Professor Ta-liang Teng
Center for Earth Sciences
University of Southern California
University Park
Los Angeles, CA 90089-0741

Professor Paul G. Richards
Lamont-Doherty Geological
Observatory of Columbia Univ.
Palisades, NY 10964

Wilmer Rivers
Teledyne Geotech
314 Montgomery Street
Alexandria, VA 22314

Dr. Clifford Thurber
State University of New York at
   Stony Brooks
Dept of Earth and Space Sciences
Stony Brook, NY 11794-2100

Professor M. Nafi Toksoz
Earth Resources Lab
Dept of Earth, Atmospheric and
   Planetary Sciences
Massachusetts Institute of Technology
42 Carleton Street
Cambridge, MA 02142

Professor Terry C. Wallace
Department of Geosciences
Building #77
University of Arizona
Tucson, AZ 85721

Weidlinger Associates
ATTN: Dr. Gregory Wojcik
4410 El Camino Real, Suite 110
Los Altos, CA 94022

Professor Francis T. Wu
Department of Geological Sciences
State University of New York
   at Binghamton
Vestal, NY 13901

Dr. Monem Abdel-Gawad
Rockwell Internat'l Science Center
1049 Camino Dos Rios
Thousand Oaks, CA 91360

Professor Shelton S. Alexander
Geosciences Department
403 Deike Building
The Pennsylvania State University
University Park, PA 16802

Dr. Ralph Archuleta
Department of Geological
   Sciences
Univ. of California at
   Santa Barbara
Santa Barbara, CA

J. Barker
Department of Geological Sciences
State University of New York
 at Binghamton
Vestal, NY   13901

Mr. William J. Best
907 Westwood Drive
Vienna, VA 22180

Dr. N. Biswas
Geophysical Institute
University of Alaska
Fairbanks, AK 99701

Dr. G. A. Bollinger
Department of Geological Sciences
Virginia Polytechnical Institute
21044 Derring Hall
Blacksburg, VA   24061

Mr. Roy Burger
1221 Serry Rd.
Schenectady, NY 12309

Dr. Robert Burridge
Schlumberger-Doll Resch Ctr.
Old Quarry Road
Ridgefield, CT 06877

Science Horizons, Inc.
ATTN: Dr. Theodore Cherry
710 Encinitas Blvd., Suite 101
Encinitas, CA 92024 (2 copies)

Professor Jon F. Claerbout
Professor Amos Nur
Dept. of Geophysics
Stanford University
Stanford, CA 94305 (2 copies)

Dr. Anton W. Dainty
AFGL/LWH
Hanscom AFB, MA 01731

Professor Adam Dziewonski
Hoffman Laboratory
Harvard University
20 Oxford St.
Cambridge, MA 02138

Professor John Ebel
Dept of Geology & Geophysics
Boston College
Chestnut Hill, MA 02167

Dr. Donald Forsyth
Dept. of Geological Sciences
Brown University
Providence, RI 02912

Dr. Anthony Gangi
Texas A&M University
Department of Geophysics
College Station, TX 77843

Dr. Freeman Gilbert
Institute of Geophysics &
   Planetary Physics
Univ. of California, San Diego
P.O. Box 109
La Jolla, CA 92037

Mr. Edward Giller
Pacific Seirra Research Corp.
1401 Wilson Boulevard
Arlington, VA 22209

Dr. Jeffrey W. Given
Sierra Geophysics
11255 Kirkland Way
Kirkland, WA 98033

Rong Song Jih
Teledyne Geotech
314 Montgomery Street
Alexandria, Virginia 22314

Professor F.K. Lamb
University of Illinois at
 Urbana-Champaign
Department of Physics
1110 West Green Street
Urbana, IL 61801

Dr. Arthur Lerner-Lam
Lamont-Doherty Geological Observatory
 of Columbia University
Palisades, NY 10964

Dr. L. Timothy Long
School of Geophysical Sciences
Georgia Institute of Technology
Atlanta, GA 30332

Dr. Peter Malin
University of California at Santa Barbara
Institute for Central Studies
Santa Barbara, CA 93106

Dr. George R. Mellman
Sierra Geophysics
11255 Kirkland Way
Kirkland, WA 98033

Dr. Bernard Minster
Institute of Geophysics and Planetary
 Physics, A-205
Scripps Institute of Oceanography
Univ. of California, San Diego
La Jolla, CA 92093

Professor John Nabelek
College of Oceanography
Oregon State University
Corvallis, OR 97331

Dr. Geza Nagy
U. California, San Diego
Dept of Ames, M.S. B-010
La Jolla, CA 92093

Dr. Jack Oliver
Department of Geology
Cornell University
Ithaca, NY 14850

Dr. Robert Phinney/Dr. F.A. Dahlen
Dept of Geological
 Geophysical Sci. University
Princeton University
Princeton, NJ 08540 (2 copies)

RADIX Systems, Inc.
Attn: Dr. Jay Pulli
2 Taft Court, Suite 203
Rockville, Maryland 20850

Dr. Norton Rimer
S-CUBED
A Division of Maxwell Laboratory
P.O. 1620
La Jolla, CA 92038-1620

Professor Larry J. Ruff
Department of Geological Sciences
1006 C.C. Little Building
University of Michigan
Ann Arbor, MI 48109-1063

Dr. Richard Sailor
TASC Inc.
55 Walkers Brook Drive
Reading, MA 01867

Thomas J. Sereno, Jr.
Service Application Int'l Corp.
10210 Campus Point Drive
San Diego, CA 92121

Dr. David G. Simpson
Lamont-Doherty Geological Observ.
 of Columbia University
Palisades, NY 10964

Dr. Bob Smith
Department of Geophysics
University of Utah
1400 East 2nd South
Salt Lake City, UT 84112

Dr. S. W. Smith
Geophysics Program
University of Washington
Seattle, WA 98195

Dr. Stewart Smith
IRIS Inc.
1616 N. Fort Myer Drive
Suite 1440
Arlington, VA 22209

Rondout Associates
ATTN: Dr. George Sutton,
Dr. Jerry Carter, Dr. Paul Pomeroy
P.O. Box 224
Stone Ridge, NY 12484 (4 copies)

Dr. L. Sykes
Lamont Doherty Geological Observ.
Columbia University
Palisades, NY 10964

Dr. Pradeep Talwani
Department of Geological Sciences
University of South Carolina
Columbia, SC 29208

Dr. R. B. Tittmann
Rockwell International Science Center
1049 Camino Dos Rios
P.O. Box 1085
Thousand Oaks, CA 91360

Professor John H. Woodhouse
Hoffman Laboratory
Harvard University
20 Oxford St.
Cambridge, MA 02138

Dr. Gregory B. Young
ENSCO, Inc.
5400 Port Royal Road
Springfield, VA 22151-2388

Dr. Peter Basham
Earth Physics Branch
Geological Survey of Canada
1 Observatory Crescent
Ottawa, Ontario
CANADA K1A OY3

Dr. Eduard Berg
Institute of Geophysics
University of Hawaii
Honolulu, HI 96822

Dr. Michel Bouchon - Universite
  Scientifique et Medicale de Grenob
Lab de Geophysique - Interne et
  Tectonophysique - I.R.I.G.M-B.P.
38402 St. Martin D'Heres
Cedex FRANCE

Dr. Hilmar Bungum/NTNF/NORSAR
P.O. Box 51
Norwegian Council of Science,
Industry and Research, NORSAR
N-2007 Kjeller, NORWAY

Dr. Michel Campillo
I.R.I.G.M.-B.P. 68
38402 St. Martin D'Heres
Cedex, FRANCE

Dr. Kin-Yip Chun
Geophysics Division
Physics Department
University of Toronto
Ontario, CANADA M5S 1A7

Dr. Alan Douglas
Ministry of Defense
Blacknest, Brimpton,
  Reading RG7-4RS
UNITED KINGDOM

Dr. Manfred Henger
Fed. Inst. For Geosciences & Nat'l Res.
Postfach 510153
D-3000 Hannover 51
FEDERAL REPUBLIC OF GERMANY

Dr. E. Husebye
NTNF/NORSAR
P.O. Box 51
N-2007 Kjeller, NORWAY

Ms. Eva Johannisson
Senior Research Officer
National Defense Research Inst.
P.O. Box 27322
S-102 54 Stockholm
SWEDEN

Tormod Kvaerna
NTNF/NORSAR
P.O. Box 51
N-2007 Kjeller, NORWAY

Mr. Peter Marshall, Procurement
  Executive, Ministry of Defense
Blacknest, Brimpton,
  Reading FG7-4RS
UNITED KINGDOM (3 copies)

Prof. Ari Ben-Menahem
Dept. of Applied Mathematics
Weizman Institute of Science
Rehovot, ISRAEL 951729

Dr. Svein Mykkeltveit
NTNF/NORSAR
P.O. Box 51
N-2007 Kjeller, NORWAY (3 copies)

Dr. Robert North
Geophysics Division
Geological Survey of Canada
1 Observatory crescent
Ottawa, Ontario
CANADA, K1A OY3

Dr. Frode Ringdal
NTNF/NORSAR
P.O. Box 51
N-2007 Kjeller, NORWAY

Dr. Jorg Schlittenhardt
Federal Inst. for Geosciences & Nat'l Res.
Postfach 510153
D-3000 Hannover 51
FEDERAL REPUBLIC OF GERMANY

University of Hawaii
Institute of Geophysics
ATTN: Dr. Daniel Walker
Honolulu, HI 96822

Dr. Ramon Cabre, S.J.
Observatorio San Calixto
Casilla 5939
La Paz Bolvia

Professor Peter Harjes
Institute for Geophysik
Rhur University/Bochum
P.O. Box 102148, 4630 Bochum 1
FEDERAL REPUBLIC OF GERMANY

Professor Brian L.N. Kennett
Research School of Earth Sciences
Institute of Advanced Studies
G.P.O. Box 4
Canberra 2601
AUSTRALIA

Dr. B. Massinon
Societe Radiomana
27, Rue Claude Bernard
7,005, Paris, FRANCE   (2 copies)

Dr. Pierre Mechler
Societe Radiomana
27, Rue Claude Bernard
75005, Paris, FRANCE

Dr. Ralph Alewine III
DARPA/NMRO
1400 Wilson Boulevard
Arlington, VA 22209-2308

Dr. Robert Blandford
DARPA/NMRO
1400 Wilson Boulevard
Arlington, VA 22209-2308

Sandia National Laboratory
ATTN: Dr. H. B. Durham
Albuquerque, NM 87185

Dr. Jack Evernden
USGS-Earthquake Studies
345 Middlefield Road
Menlo Park, CA 94025

U.S. Geological Survey
ATTN: Dr. T. Hanks
Nat'l Earthquake Resch Center
345 Middlefield Road
Menlo Park, CA 94025

Dr. James Hannon
Lawrence Livermore Nat'l Lab.
P.O. Box 808
Livermore, CA 94550

Paul Johnson
ESS-4, Mail Stop J979
Los Alamos National Laboratory
Los Alamos, NM 87545

Ms. Ann Kerr
DARPA/NMRO
1400 Wilson Boulevard
Arlington, VA 22209-2308

Dr. Max Koontz
US Dept of Energy/DP 5
Forrestal Building
1000 Independence Ave.
Washington, D.C. 20585

Dr. W. H. K. Lee
USGS
Office of Earthquakes, Volcanoes,
  & Engineering
Branch of Seismology
345 Middlefield Rd
Menlo Park, CA 94025

Dr. William Leith
USGS
Mail Stop 928
Reston, VA 22092

Dr. Richard Lewis
Dir. Earthquake Engineering and
  Geophysics
U.S. Army Corps of Engineers
Box 631
Vicksburg, MS 39180

Dr. Robert Masse'
Box 25046, Mail Stop 967
Denver Federal Center
Denver, Colorado 80225

Richard Morrow
ACDA/VI
Room 5741
320 21st Street N.W.
Washington, D.C. 20451

Dr. Keith K. Nakanishi
Lawrence Livermore National Lab
P.O. Box 808, L-205
Livermore, CA 94550 (2 copies)

Dr. Carl Newton
Los Alamos National Lab.
P.O. Box 1663
Mail Stop C335, Group E553
Los Alamos, NM 87545

Dr. Kenneth H. Olsen
Los Alamos Scientific Lab.
Post Office Box 1663
Los Alamos, NM 87545

Howard J. Patton
Lawrence Livermore National
  Laboratory
P.O. Box 808, L-205
Livermore, CA 94550

Mr. Chris Paine
Office of Senator Kennedy
SR 315
United States Senate
Washington, D.C. 20510

AFOSR/NP
ATTN: Colonel Jerry J. Perrizo
Bldg 410
Bolling AFB, Wash D.C. 20332-6448

HQ AFTAC/TT
Attn: Dr. Frank F. Pilotte
Patrick AFB, Florida 32925-6001

Mr. Jack Rachlin
USGS - Geology, Rm 3 C136
Mail Stop 928 National Center
Reston, VA 22092

Robert Reinke
AFWL/NTESG
Kirtland AFB, NM 87117-6008

HQ AFTAC/TGR
Attn: Dr. George H. Rothe
Patrick AFB, Florida 32925-6001

Donald L. Springer
Lawrence Livermore National Laboratory
P.O. Box 808, L-205
Livermore, CA 94550

Dr. Lawrence Turnbull
OSWR/NED
Central Intelligence Agency
CIA, Room 5G48
Washington, D.C. 20505

Dr. Thomas Weaver
Los Alamos National Laboratory
P.O. Box 1663
MS C335
Los Alamos, NM 87545

AFGL/SULL
Research Library
Hanscom AFB, MA 01731-5000 (2 copies)

Secretary of the Air Force (SAFRD)
Washington, DC 20330
Office of the Secretary Defense
DDR & E
Washington, DC 20330

DARPA/RMO/Security Office
1400 Wilson Blvd.
Arlington, VA 22209

HQ DNA
ATTN: Technical Library
Washington, DC 20305

AFGL/XO
Hanscom AFB, MA 01731-5000

AFGL/LW
Hanscom AFB, MA 01731-5000

DARPA/PM
1400 Wilson Boulevard
Arlington, VA 22209

Defense Technical
 Information Center
Cameron Station
Alexandria, VA 22314
(5 copies)

Defense Intelligence Agency
Directorate for Scientific &
 Technical Intelligence
Washington, D.C. 20301

Defense Nuclear Agency/SPSS
ATTN: Dr. Michael Shore
6801 Telegraph Road
Alexandria, VA 22310

AFTAC/CA (STINFO)
Patrick AFB, FL 32925-6001

Dr. Gregory van der Vink
Congress of the United States
Office of Technology Assessment
Washington, D.C. 20510

Mr. Alfred Lieberman
ACDA/VI-OA'State Department Building
Room 5726
320 - 21St Street, NW
Washington, D.C. 20451

TACTEC
Battelle Memorial Institute
505 King Avenue
Columbus, OH 43201 (Final report only)

DARPA/RMO/RETRIEVAL
1400 Wilson Boulevard
Arlington, VA 22209